UNIVERSITY OF CALIFORNIA,
IRVINE

Mechanical and genetic tools for micropatterning cells

DISSERTATION

submitted in partial satisfaction of the requirements
for the degree of

DOCTOR OF PHILOSOPHY

in Biomedical Engineering

by

David Jiang Li

Dissertation Committee:
Professor Elliot E. Hui, Chair
Professor Chang C. Liu
Professor Jered B. Haun

2018

DEDICATION

To my mom and dad.

Your sacrifices and hard work have paved my path and made possible every fortune I enjoy.

And to my sister, Ann.

You've taught me there's always room to make the world a better place, and the best way is to start with yourself.

Table of Contents

List of Figures

List of Tables

ACKNOWLEDGMENTS

Funding for my training and the work in this dissertation was provided by a NSF "LifeChips" IGERT training fellowship, the NSF I/UCRC Center for Advanced Design and Manufacturing of Integrated Microfluidics(CADMIM), the Center for Complex Biological Systems (CCBS) at UCI, and a DARPA Young Faculty Award, and multiple Teaching Assistantships in the BME department.

It has been a great privilege to work with a number of collaborators spanning many fields. Thank you to:

- Dr. Monica Kim, Long Pham, and Dr. Brandon Wong, who initiated work on microporous membrane fabrication.
- Prof. Olivier Cinquin for motivating the *C. elegans* filtering work, Dr. Evan Lister for help with handling the worms and running lifespan experiments, and Michael Corrado for assistance with prototyping flow devices.
- Dr. Virginia Pensebene and Dr. Juan Gnecco, for the endometrial perivascular stroma model.
- Dr. Krysten Jones, Dr. Will Porterfield, and Prof. Jennifer Prescher for the split-luciferase work.
- Kamran Ali, for building up our lab's expertise in optogenetics from scratch, and mentoring me through the Phytochrome work.
- Dr. Evan Olson, for sharing schematics and advice on building the LED array.
- Dr. Jutta Dalton, for advice on light-activated yeast two-hybrids.
- Allison Curtis, for the work on the reconfigurable elastic substrates, and Justin Do, for help with establishing early patterning techniques.
- Katie Cabral, Prof. Zev Gartner, and Dr. Michael Todhunter for providing reagents and tremendously helpful advice for setting up DNA-patterned cell adhesion.
- Dr. Rie Nakajima and Dr. Algimantas Jasinskas from Professor Philip Felgner's group for their expertise and help in microspotting DNA.
- The Khine lab, for graciously allowing me to use so many of their rapid prototyping tools.
- The staff of the INRF, BiON, and LEXI facilities, in particular Jake Hes and Richard Chang for their diligence over the years.

I am deeply grateful for the support and mentorship of my advisor, Professor Elliot Hui. I've personally benefited tremendously from his infectious enthusiasm for science and the sincere empathy he has for all his trainees. Through every setback he has been patient and constructive, and he celebrated every success by inspiring courage to push for more.

I'm also thankful for the opportunities Elliot and the other BME faculty have provided me in developing as an educator. My experiences working together with extraordinarily talented and driven students both in the lab and the classroom were among the most rewarding for me in my time at UCI.

Thank you also to all my incredible labmates who have made working at NS2 so enjoyable and fulfilling. I've been fortunate to not only learn from the best engineers and biologists, but also grow together with the best people.

Having so many friends at UCI both in and out of the lab was a true blessing. Taking midnight hikes in the hills by campus, grilling summer peaches at sunset, racing bikes up Newport Coast, and cocktail parties both hosted and crashed - these and so many other good memories will stay with me forever. But I've also been humbled to find how much the small moments have stuck as well. I am indebted to so many of you for all the compassionate support and heartfelt friendship you have shown me – thank you.

Lastly, thank you Elena Liang, for being an endless source of joy and comfort. I am grateful for all that you do for me and the unmatched happiness you have brought into my life.

CURRICULUM VITAE

David Jiang Li

EDUCATION

Doctor of Philosophy in Biomedical Engineering **2018**
University of California, Irvine

Masters of Science in Biomedical Engineering **2015**
University of California, Irvine

Bachelor of Science in Bioengineering **2009**
University of California, Berkeley

RESEARCH EXPERIENCE

Graduate Research Assistant **2010–2018**
University of California, Irvine

TEACHING EXPERIENCE

Teaching Assistant **2012–2018**
University of California, Irvine

Cell and Molecular Engineering I	*Winter 2014, 2018*
Cell and Molecular Engineering II	*Spring 2015, 2016, 2017*
Engineering Analysis and Design I	*Fall 2012, 2016, 2017*
Engineering Analysis and Design II	*Winter 2013*
Organ Transport Systems	*Winter 2016*

REFEREED JOURNAL PUBLICATIONS

Compartmentalized Culture of Perivascular Stroma and Endothelial Cells in a Microfluidic Model of the Human Endometrium. **2017**
Annals of Biomedical Engineering.

Patterning of sharp cellular interfaces with a reconfigurable elastic substrate. **2016**
Integrative Biology.

Visualizing cell proximity with genetically encoded bioluminescent reporters. **2015**
ACS Chemical Biology.

Microfabricated of high-resolution porous membranes for cell culture. **2014**
Journal of Membrane Science.

Microfabricated of high-resolution porous membranes for cell culture. **2014**
Journal of Membrane Science.

ABSTRACT OF THE DISSERTATION

Mechanical and genetic tools for micropatterning cells

By

David Jiang Li

Doctor of Philosophy in Biomedical Engineering

University of California, Irvine, 2018

Professor Elliot E. Hui, Chair

Intercellular communication is a fundamental driver of tissue function across developing, mature, as well as diseased organ systems. We have developed a variety of tools for controlling the patterning of cells at the microscale, each enabling experiments targeting different aspects of cell communication.

Organ-on-a-chip models often reconstitute tissue interfaces across a porous membrane that is intended to maintain compartmentalization of different cell layers while preserving cell-cell interactions. However, such membranes are typically substantially thicker and exhibit lower porosity than natural basement membrane. We optimized a photolithographic process in 1002F epoxy resin to produce thin microporous membranes with good biocompatibility, optical transparency, and low auto-fluorescence. Characterization of fabrication limits by profilometry and SEM show we are able to produce membranes under 1 μm in thickness with pores as small as 0.8 μm. Cells seeded on either side of the membrane can interact through the pores but do not migrate across. 1002F membranes were employed to divide a two-chambered microfluidic model system of perivascular endometrial stroma, which successfully recapitulates decidualization in response to combined progesterone and oestrogen treatment. This model could potentially be applied to screening for drug toxicity effects on endometrial tissue, which remains an under explored area of women's health.

Secondly, micropatterning of planar co-cultures can achieve precise organization suitable for optimized organ models or the study of developmental processes. We devised a reconfigurable elastomeric substrate to pattern a very clean boundary interface between two cell populations. This system has been employed to recapitulate morphogen gradients in vitro. A significant limitation shared across most cell micropatterning approaches is the inability to pattern more than two populations. We adopted a DNA-programmed cell adhesion technique to extend patterning to three or more cell populations. This approach combines the incorporation of short DNA oligomers onto cell surfaces with glass substrates patterned with complimentary DNA. Using two different pairs of DNA compliments allowed patterning of two different cell types onto different regions of a single substrate, with less than 5% cross contamination. We also demonstrate the feasibility of a simple microfluidic approach to immobilizing DNA on glass with μm-scale resolution over cm-scale areas without the use of expensive micropatterning instruments. Expanding the number of patterned cell types may improve the physiological relevance of in vitro models of complex organ systems such as the liver.

Finally, we establish a platform for engineering the photoswitchable protein interaction of PhyB and PIF for optogenetic control of gene expression, with the goal of patterning cell phenotype using light. Exposure to 650nm red light induces PhyB and PIF to interact, while 750nm far-red light drives their dissociation. We tied PhyB-PIF interaction to reporter gene expression in a yeast two-hybrid assay and studied the relationship between red light pulse duration and induced gene expression using a programmable LED array. We also present work towards engineering this response through altering subcellular localization of the PIF component, which could allow encoding distinct responses by tuning pulse length.

Chapter 1

Fabrication of microporous membranes in 1002F epoxy resin

1.1 Introduction

Organ on chip devices are useful for their ability to recapitulate key physiological process of interest to human health in an in vitro format which is amenable to high-throughput screening. This can result in improved predictive power relative to traditional in vitro cell culture models, at lower cost relative to animal model systems. [1]. Thin membranes with pores smaller than cells are employed in these devices for compartmentalizing two cell populations while allowing some degree of interaction between them, imitating the role of basement membrane between different tissue layers in natural organ systems. For example, in a model of lung tissue an elastomeric membrane has been used to compartmentalize lung fibroblasts and epithelial cells into two chambers, allowing the formation of an air-liquid interface [2]. Usefully, the elastic membrane enabled cyclical application of strain

found reveal harmful effects of exposure to silica nanoparticles not found in the absence of mechanical forces.

However, the micro-molding fabrication process used to produce these elastic membranes cannot easily produce membrane thicknesses under 10μm [3]. Other processes which are able to produce membranes closer to the 1 μm thickness of natural basement membrane have other limitations. Track-etching with high energy ion bombardment, a process commonly used to produce porous membranes for commercially available transwell inserts, results in random pore placement [4]. This causes membranes above a certain porosity, typically around 5% or less, to contain overlapping pores with larger effective dimensions than intended. Other processes such as E-beam lithography have been applied to fabricating ordered arrays of pores in a $<$1 μm thick silicon nitride membrane, but the serial natural of this process limits total membrane area [5].

To address these limitations, we developed a process for photolithographic fabrication of porous membranes in 1002F. Photosensitized Epon epoxy resin 1002F was originally developed as a negative-tone photoresist for applications requiring low autofluorescence and good biocompatibility [6]. By further adjusting photoresist composition and fabrication process parameters, we were able to decrease the minimum membrane thickness in 1002F from 10μm to 1μm and produce ordered arrays of pores with diameters approaching the diffraction limit of photopatterning. Release and handling of the delicate membranes produced in this process were facilitated by the addition of a sacrificial release layer and plastic adhesive reinforcements, respectively. Membrane thickness, pore size distribution, and optical imaging properties of the 1002F membranes were characterized. Finally, in collaboration with the VIIBRE center at the Vanderbilt University, porous 1002F membranes were successfully integrated into a functional compartmentalized two-chamber model of endometrial perivascular tissue.

1.2 Fabrication Process

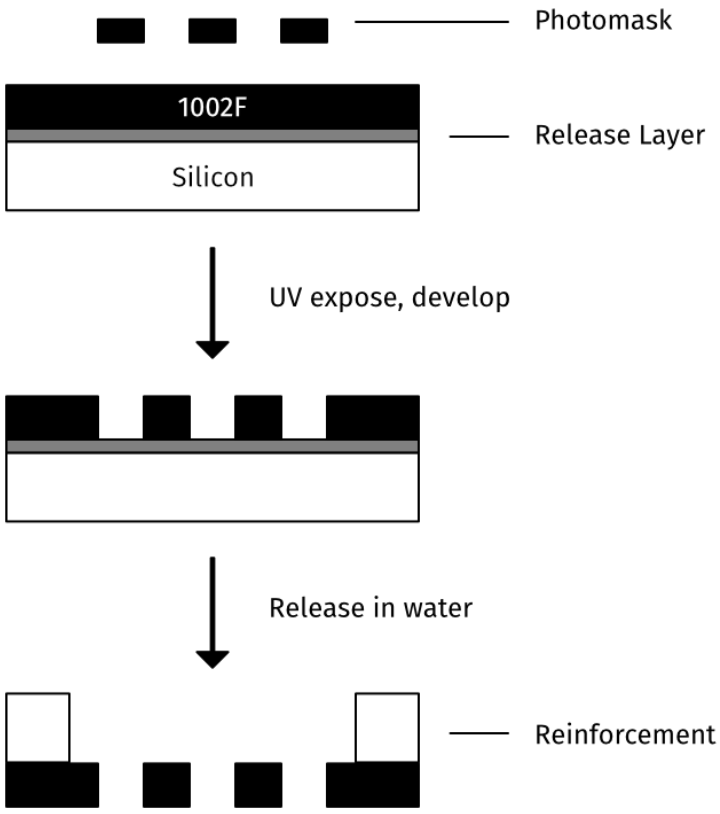

Figure 1.1: Schematic of 1002F membrane fabrication process.

The fabrication process,summarized in [7], is described in detail below. Photomasks to specify pore size and layout are designed using the layout software, kic, freely available from Whiteley Research (http://www.wrcad.com/freestuff.html). Features smaller than about 8 μm require the use of a chrome mask (Photronics, Brookfield CT). Pore geometry is A silicon wafer serves as the base substrate, onto which a sacrificial release layer is deposited by spin-coating. 1002F photoresist is then added and spun to set the desired thickness for the final membrane. The resist is set by evaporating excess solvent in a two-step bake: 10 minutes at 65°C followed by 20 minutes at 95°C. The wafer is then exposed to UV through a photomask before repeating the same two-step bake to set the UV cross-linked areas. Non-crosslinked photoresist is removed by immersing the wafer in a development bath of

propylene glycol methyl ether acetate (PGMEA), followed by a rinse in isopropyl alcohol (IPA) and drying under a compressed nitrogen stream. Mechanical reinforcements can then be applied if required before releasing the finished membranes from the silicon substrate by immersion in a bath of distilled water. Details for each process step follow below.

1.2.1 Photoresist mixing

Component quantities for 1002F photoresist formulations targeting various final layer thicknesses are listed in Table 1.1. 1002F resin (Miller-Stephenson, Sylmar CA) and the photoinitiator, triarylsulfonium hexafluoroantimonate mixed salts in 50 wt. % in propylene carbonate (Sigma-Aldrich), are commercially available. The gamma-Butyrolactone (GBL) solvent (Sigma-Aldrich) is a controlled substance and requires authorization for purchase and storage.

Table 1.1: 1002F Component Ratios

Component	1002F-1	1002F-10	1002F-50
1002F Resin	196 g	196 g	244 g
Photoinitiator	19.6 g	19.6 g	24.4 g
GBL	584.4 g	184.4 g	131.6 g
Total	800 g	400 g	400 g

To mix, components are combined in a glass beaker and stirred using a photoresist mixer graciously shared by Dr. Richard Chang at 300 rpm for 16 hours in a class 10,000 cleanroom environment. Mixed photoresists can be stored in tightly sealed amber glass bottles protected from light for at least 6 months.

1.2.2 Release layer

A solution of 2% Micro-90 (International Products, Burlinton, NJ) was found to provide both good adhesion for the 1002F photoresist through all processing steps as well as reliable, gentle release in a water bath. Higher percentages of soap were found to result in particulates on the surface of the wafer, causing streaks to form upon later spin-coating photoresist. Spinning the Micro-90 release layer in two stages (first at low speed to promote even coverage, and second at higher speed to dry a thin layer on the wafer surface) was not found to be more reliable than a single high speed spin, but was retained for practical convenience when programming the spin-coater.

1.2.3 Spin coating photoresist

The final membrane thickness will mostly be determined by the viscosity of the 1002F photoresist mixture and the parameters used during its spin-coating step. Spin-coating in two stages is helpful in achieving uniform thickness across the entire wafer area. The first spin step, typically at 500 rpm for 10 seconds, helps promote even coverage of the wafer by allowing the resist to spread under low centrifugal force.

Applying the higher centrifugal force in the second step for a longer period of time, typically 40 seconds, allows the membrane to approach a final thickness as dictated by the spin-coat thickness equation (eq. 1.1), where t is the membrane thickness and ω is the rotational spin speed.

$$t \propto \frac{1}{\sqrt{\omega}} \tag{1.1}$$

Empirical measurements of the membrane thickness obtained from a variety of resist compositions and different spin speeds are summarized in Table 1.2.

Table 1.2: 1002F Membrane Thickness

Spin speed	1002F-1	1002F-10	1002F-50
2000 rpm	4 μm	35 μm	50 μm
5000 rpm	1 μm	8 μm	35 μm

1.2.4 UV Exposure

Photocrosslinking of the 1002F photoresist was performed using a MA6 mask aligner (Suss Microtech) in low-vacuum mode. Optimal exposure times will depend on resist thickness and were found to vary with pore size. Typical parameters used for 1 μm thick membranes were between 6 and 15 seconds at 10 mW/cm^2 lamp intensity.

Photopatterning lower resolution patterns in thicker (>10 μm) 1002F was performed with UV flood exposure (Oriel Instruments), with 25 seconds at 14 mW/cm^2 being typical for 50 μm thick resist layers.

1.3 Multilayer Fabrication

Multiple layers of 1002F photoresist can be built up on a single substrate, exposing each layer to define a pattern of crosslinking before the next layer is added. UV light exposure through photomasks used to pattern upper resist layers can also penetrate into layers below, cross-linking regions which were not cross-linked during previous patterning steps. This can be used to produce an integrated support lattice, with thin layers of small pores supported by a thicker overlaid layer.

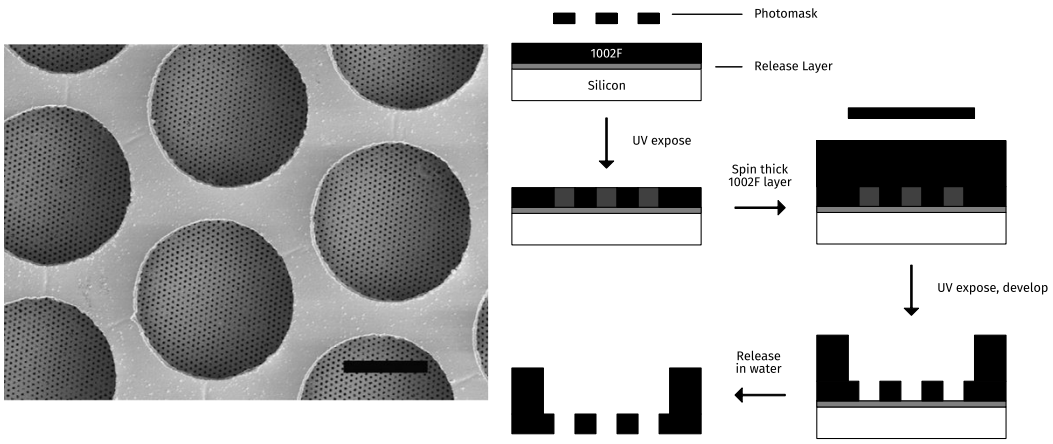

Figure 1.2: Two-layer 1002F process summary
Left: SEM micrograph of 2-layer 1002F membrane consisting of 1 μm thick layer patterned with .8 μm diameter pores reinforced by a 35 μm thick layer patterned with 100 μm diameter pores. Scale bar: 50 μm. Right: Summary of 2-layer fabrication process.

1.4 Pore Size Uniformity

Membrane pore sizes and porosity were measured using scanning electron microscopy (SEM). Samples were mounted onto standard SEM stubs using carbon tape and were sputter-coated with a thin layer of iridium using a Model IBS/e Ion Beam Sputter Depositing and Etching System (South Bay Technology, San Clemente, CA). Images were captured at various magnifications using a Magellan 400 XHR SEM (FEI, Hillsboro, OR). A custom MATLAB (MathWorks) program was used to quantify pore size and porosity from the SEM images.

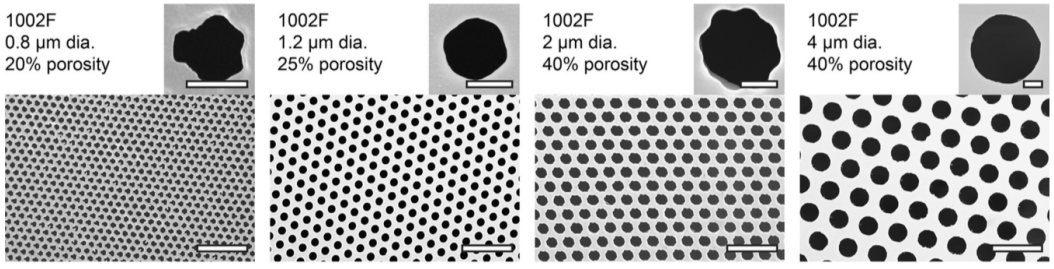

Figure 1.3: SEM micrographs of 1 μm thick 1002F membranes.
Scale bars: 1μm (insets) or 10μm (wide field)

Table 1.3: 1002F pore size uniformity.

All measurements taken from 1 μm thick membranes. Mean $\pm$ Standard Deviation taken from a single representative membrane sample

Mask pore size	Measured pore size
0.8 μm	1.04 $\pm$ .03 μm
1.2 μm	1.35 $\pm$ .04 μm
2.0 μm	2.00 $\pm$ .09 μm
4.0 μm	3.91 $\pm$ .03 μm

As membrane thickness increases, the minimum resolvable feature size is expected to also increase. We are able to achieve a maximum 1:4 aspect ratio, properly resolving mask features in layers that are at most 4 times thicker than the critical feature size.

At the smallest pore sizes, the Manhattan-geometry used to draw the chrome-photomask results in pores which are not perfectly circular.

1.5 Quality of Cell Imaging on Membranes

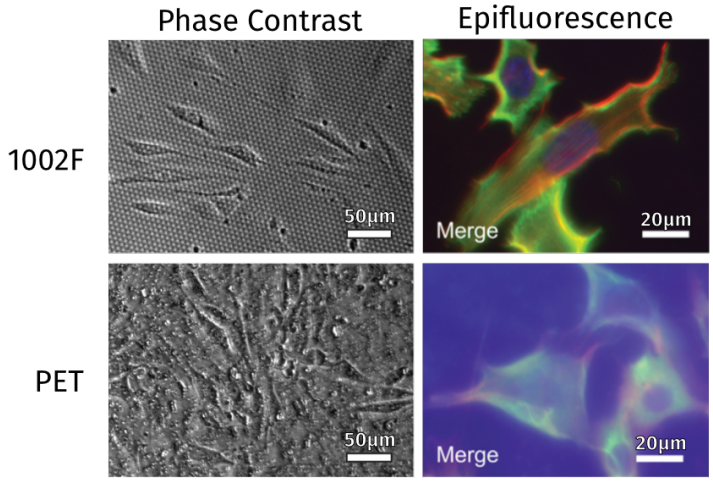

Figure 1.4: Phase contrast and epifluorescence imaging on 1002F vs. PET membranes. Fluorescence images are composites of three stains: alpha-Vinculin in green, Laminin in red, and Hoescht nuclear stain in blue. Scale bars: 20μm. Images courtesy of Monica Kim.

In addition to previously mentioned advantages, the optical properties of 1002F membranes for cell imaging are also improved over commercially available materials commonly used in transwell inserts, such as PET. Phase contrast imaging, the gold standard for evaluating cell morphology, yields distorted and unclear images on commercial track-etched PET membranes. This distortion is significantly reduced in 1002F membranes, as seen in Figure 1.4. 1002F also exhibits lower autofluorescence, particularly in UV-excitation blue-emission channels, giving better visualization of DNA stains or other fluorescent reporter signals. Relative auto- fluorescence of porous membranes made of Parylene HT (1 μm), 1002F (1 μm), polyethylene terephthalate (PET, 9 μm), and polycarbonate (PC, 10 μm) were measured using on a Nikon Eclipse TE200 epifluorescence microscope using a 40x objective lens and 100 W mercury arc lamp source (Osram). A standard polystyrene dish (PS, 670 μm) is also included for comparison. The following filters were used for each fluorescence channel: UV-2E/C (DAPI channel, excitation [ex]: 340– 380 nm, emission [em]: 435–485 nm), B-2E/C (FITC channel, ex: 465–495 nm, em: 515–555 nm), and G-2E/C (TRITC channel, ex: 528–553 nm, em: 590–650 nm). Images were collected with the following exposure times: 500 ms for DAPI, 5 s for TRITC, and 5 s for FITC. The PET membrane sample was imaged for only 70 ms in the DAPI channel due to oversaturation at 500 ms; the measured values were scaled for plotting assuming a linear relationship between signal and imaging time and normalized to the autofluorescence of a glass slide. These readings do not indicate the inherent autofluorescence of these materials since the thicknesses are not the same, but are indicative of practically observed autofluorescence when imaging cells on these substrates. Note that Parylene and 1002F membranes are comparable to commercial PC membranes and significantly better than the PET and PS substrates in terms of autofluorescence. These measurements are summarized in Figure 1.5.

1.6 Application to in vitro endometrial co-culture model

1002F membranes have successfully been integrated into an in vitro co-culture model of endometrial perivascular tissue [8]. The primary goal of this model was to recapitulate the decidualization response of endometrial tissues in response to ovarian hormones oestrogen and progesterone. A two-chambered design was used to enable controlled media delivery to each cell type independently, as well as independent biochemical analysis of secreted paracrine and endocrine signals.

In this model, a 6 μm thick 1002F membrane patterned with 2μm diameter pores at 10% porosity was integrated into a microfluidic flow chamber device to partition separate top and bottom chambers each with their own flow inlet and outlet. Primary fibroblasts isolated from donor endometrial tissue were seeded on one side of the membrane and human umbilical vein endothelial cells (HUVECs) were seeded on the other side.

The ability of the seeded coculture to form a confluent barrier to diffusion between the two chambers was confirmed by measuring the transfer of fluorescently labeled dextran (150 kD MW). The measured permability coefficient in devices seeded with endothelial-stroma co-culture was significantly reduced relative to unseeded devices.

Biological responses of the perviascular co-culture to endocrine signaling were examined by mimicking the oestrogen and progesterone changes that accompany the transition from proliferative to secretory phase in vivo. When exposed to both oestrogen (1 nM 17-β -oestradiol, E2, in DMEM) and the synthetic progesterone analog medroxyprogesterone acetate (MPA, .5 mM), over 14 days, secreted prolactin as assayed by ELISA on collected flow-through media from the device outlet was found to be increased relative to co-cultures exposed to oestrogen alone. Further, over an additional 14 days in culture, fibroblasts exposed to both E2 and MPA were found to adopt a cuboidal morphology typical to decidualizing stroma in vivo, while fibroblasts treated only with E2 remained in a spindle-like shape. This demon-

strates the capability of the model to maintain culture over a full 28-day menstrual cycle, and mimic responses to hormonal phases with continuous sampling capabilities for quantitative biochemical analysis.

1.7 Conclusion

The direct photolithographic fabrication process developed here produces membranes of 1-50+ μm thickness with controlled pore placement at up to 40% total porosity. The minimum achievable pore size is as small as .25 times the thickness of the membranes, limited to roughly 1 μm in diameter in thinner membranes by diffraction limit of UV light used for photo-crosslinking. The biocompatibility and low autofluorescence of the 1002F resin support long-term cell culture on one or both faces of the membrane. These membranes can be integrated into microfluidic flow chamber devices to compartmentalize two cell types, allowing their interaction through the membrane. Delivery of nutrients and signaling factors to each chamber can be controlled independently, and secreted metabolites of each cell type analyzed separately. An endometrial perivascular model applying this approach successfully recapitulated decidualization of endometrial stroma, which can have clinical relevance for screening compounds which affect these aspects of reproductive health. Physical compartmentalization is useful to a number of other organ-on-chip models, such as Blood-brain barrier models which require the establishment of a tight epithelial layer. Results from our 1002F membranes in successfully maintaining a tight diffusive barrier when seeded with cells is encouraging evidence that they could also support the tight cell packing required to produce a high Trans-Epithelial Electrical Resistance (TEER) in astrocyte-epithelial cell co-culture.

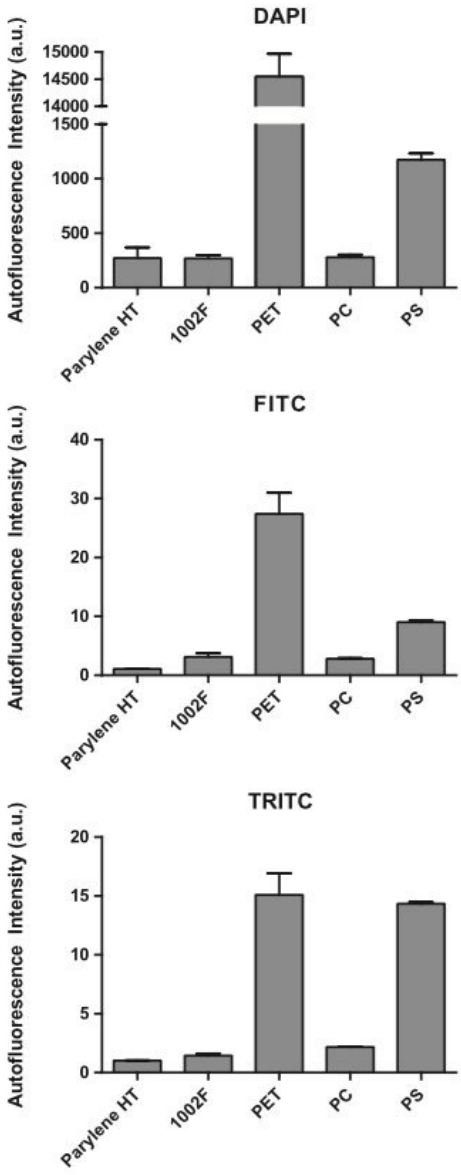

Figure 1.5: Relative Autofluorescence of Porous Membranes
Error bars are standard error of the mean across three membrane samples

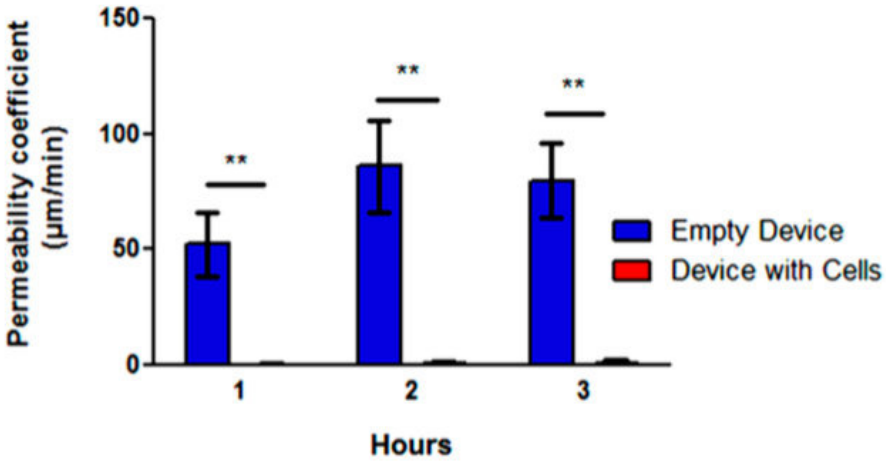

Figure 1.6: Permeability of FITC-Dextran in two-chambered device under flow (2.5μL/min) (**: p = 0.0098)

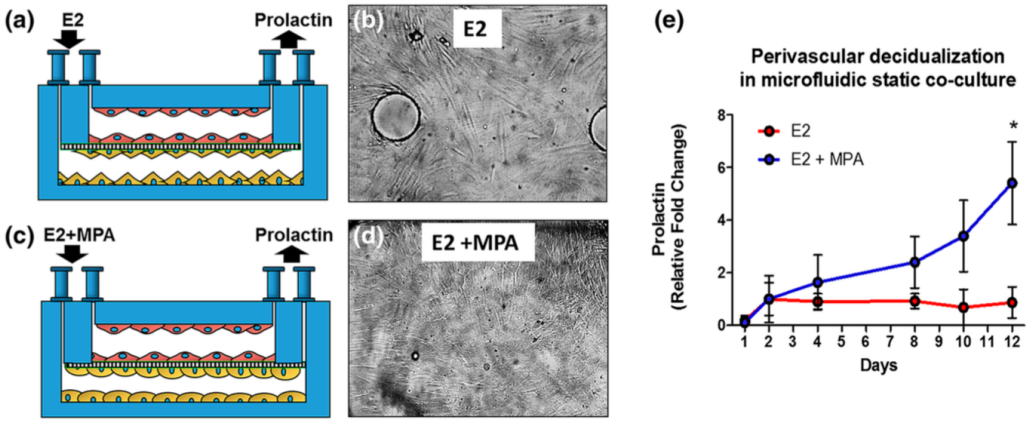

Figure 1.7: Physiological response of the perivascular stroma model to endocrine cues (a,c) Schematic of the experimental design for measuring responses to endocrine signals. (b,d) Bright field image of co-cultures showing changes of morphology for stroma from fibroblast-like to cuboidal shape in response to combined E2 and MPA only. (e) Prolactin (PRL) production measured by ELISA increases over time under the influence of E2 + MPA, but not when cultured with E2 alone (*: p $<$ 0.05).

Bibliography

[1] S. N. Bhatia and D. E. Ingber, "Microfluidic organs-on-chips," aug 2014.

[2] D. Huh, B. D. Matthews, A. Mammoto, M. Montoya-Zavala, H. Yuan Hsin, and D. E. Ingber, "Reconstituting organ-level lung functions on a chip," *Science*, vol. 328, pp. 1662–1668, jun 2010.

[3] E. Ostuni, R. Kane, C. S. Chen, D. E. Ingber, and G. M. Whitesides, "Patterning mammalian cells using elastomeric membranes," *Langmuir*, vol. 16, no. 20, pp. 7811–7819, 2000.

[4] H. H. Chung, M. Mireles, B. J. Kwarta, and T. R. Gaborski, "Use of porous membranes in tissue barrier and co-culture models," jun 2018.

[5] S. H. Ma, L. A. Lepak, R. J. Hussain, W. Shain, and M. L. Shuler, "An endothelial and astrocyte co-culture model of the blood-brain barrier utilizing an ultra-thin, nanofabricated silicon nitride membrane," *Lab on a Chip*, vol. 5, pp. 74–85, dec 2005.

[6] J. H. Pai, Y. Wang, G. T. A. Salazar, C. E. Sims, M. Bachman, G. P. Li, and N. L. Allbritton, "Photoresist with low fluorescence for bioanalytical applications," *Analytical Chemistry*, vol. 79, no. 22, pp. 8774–8780, 2007.

[7] M. Y. Kim, D. J. Li, L. K. Pham, B. G. Wong, and E. E. Hui, "Microfabrication of high-resolution porous membranes for cell culture," *Journal of Membrane Science*, vol. 452, pp. 460–469, 2014.

[8] J. S. Gnecco, V. Pensabene, D. J. Li, T. Ding, E. E. Hui, K. L. Bruner-Tran, and K. G. Osteen, "Compartmentalized Culture of Perivascular Stroma and Endothelial Cells in a Microfluidic Model of the Human Endometrium," *Annals of Biomedical Engineering*, 2017.

Chapter 2

Tools for patterning planar co-cocultures

2.1 Introduction

Heterogeneity at the micro-scale is understood to play an important role in cell function. For screening of drugs in *in vitro* models, recreating this micro-scale heterogeneity is then potentially important to accurate prediction of *in vivo* responses. In liver models, for example, previous work has shown structured co-cultures of hepatocytes and fibroblasts results in higher levels of liver-specific function as evaluated by albumin and urea secretion and CYP450 enzyme activity. These are also maintained for longer periods of time when compared to mixed unstructured co-culture of the same two cell types [1]. Experimental control at the micro-scale can also enable experiments which improve our understanding of the nature of cell interactions which are responsible for these effects. For instance, reconfigurable co-culture experiments demonstrate the increased liver function from hepatoyte-fibroblast co-culture is dependent on an initial period of contact-dependent interaction between the two cell types, yet can be later maintained through soluble-factor signaling alone without

contact [2]. This suggests the nature of intercellular interactions responsible for maintaining liver function in hepatocytes are potentially dynamic and bidirectional.

No single cell-patterning device or strategy is equally useful to all experiments; the opaque silicon construction of the reconfigurable comb devices described above requires the use of less-common upright microscopes for imaging, and the additional steps required limit their use for high-throughput screening. We address these issues by designing a simple alternative using a self-healing cut in a transparent elastomeric substrate and demonstrate its application to patterning a clean contacting interface between two cell types and following their interaction by live imaging. To enable the study of paracrine signaling interactions which may not require direct contact and occur over longer, mm length scales, we adapted a simple stenciling approach, using rapid fabrication to quickly produce a range of patterns with varied distance between two cell types in a single well. Finally we extend patterning to more than two cell types by adopting a synthetic DNA-programmed scheme for specifying cell adhesion and extend the approach by enabling microfluidic patterning of large connected regions of immobilized DNA.

2.2 Patterning a contacting interface with reconfigurable elastomeric substrate

A clean interface between two cell types is important for studying intercellular signaling processes which depend on a combination of direct contact-mediated and secreted paracrine signaling. New synthetic in vitro models of morphorgen gradient formation, for example, are useful for studying the

Figure 2.2 shoes a comparison of co-culture interfaces produced by different patterning methods. In sequential cell seeding, with on cell type seeded to only half a well and a second

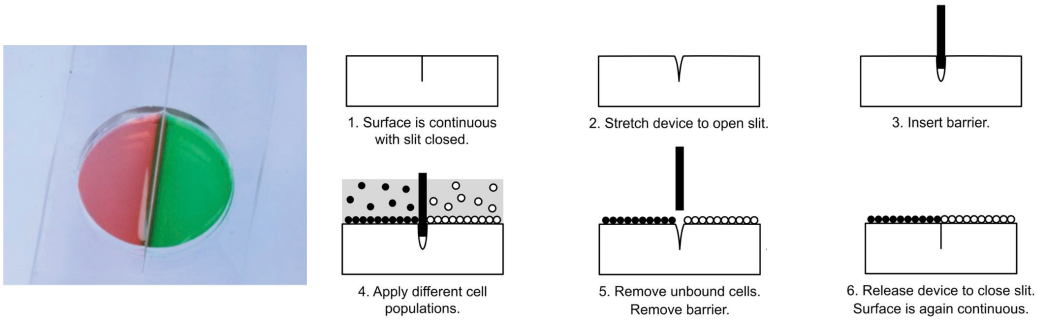

Figure 2.1: Schematic of reconfigurable elastic substrates

cell type seeded on top, significant cross-contamination can occur. A commercial barrier device such as the Ibidi chambers intended for wound healing and migration assays can allow simultaneous seeding of two cell populations. However the barrier leaves a gap of several hundred microns between the two populations. Following barrier removal the two populations can migrate together as in a wound healing assay but the sharpness of the interface may be considerably degraded. Simultaneous seeding on the reconfigurable elastic substrate following the scheme outlined in Figure 2.1 produces a sharp contact interface between two cell populations with minimal cross-contamination.

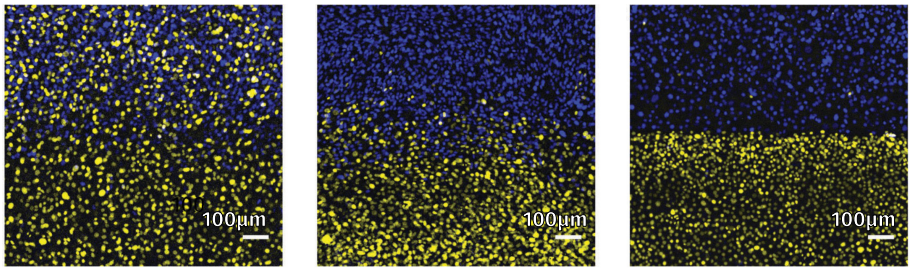

Figure 2.2: Comparison of seeding techniques to produce a contact interface
Blue: 3T3 cells expressing mTurquoise. Yellow: 3T3 cells expressing Citrine. All scale bars = 100 mm.

The depth of cut was found to be important to quality of cell patterns produced: if the slit was cut too shallow, cell adhesion was poor in the vicinity of the slit (Fig 2.3), possibly due to compressive deformation of the PDMS around the barrier. A machined acrylic rig was used to hold a razor blade and produce cuts of repeatable depth.

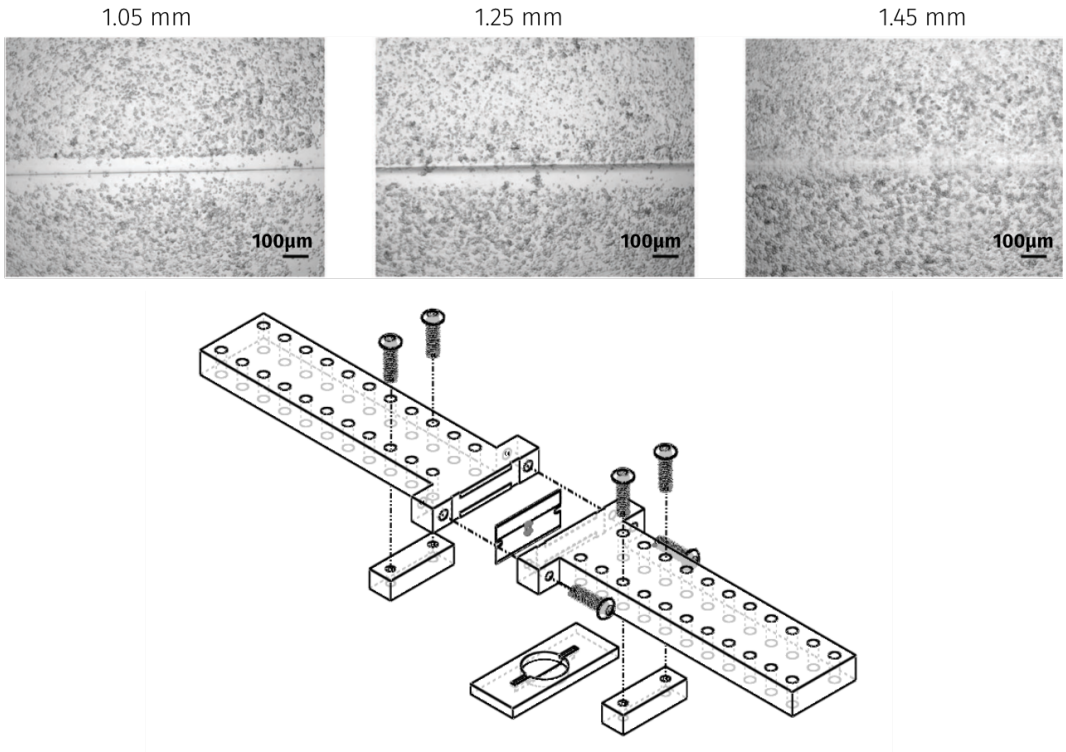

Figure 2.3: Effects of depth of cut on cell seeding quality
Top: NMUMG cells seeded on reconfigurable elastic substrates cut to different depths; shallow cuts result in cell detachment near the cut. Bottom: acrylic cutting rig to generate reproducible cut depths. Depth of cut is adjusted by adding or removing thin spacers between the rectangular "feet' and main body of the rig.

2.3 Patterning with laser-cut stencils

Cell patterns can be generated simply through the use of stencils to create physically separated wells into which different adherent cell types can be seeded. Through the use of micromolds produced by soft-lithography, cell patterns of [3] For study of long-range paracrine signaling with mm-scale length scales, cell patterns can be generated . Using a laser cutter to create custom stencils allows rapid creation and redesign of the shape and distance of cell islands patterned in this manner.

2.3.1 Application to Split-Luciferase Cell Distance Reporter

Jen Prescher's lab in Chemistry at UCI developed a genetically encoded reporter for distance between two cell populations. The system entails a split *Gaussia* luciferase (Gluc) enzyme, with each half expressed as a secreted protein in a different cell population. The N-terminal Gluc fragment is fused to Jun, and C-terminal Gluc is fused to Fos. Fos-Jun interaction drives reconstitution of the split-Gluc, which otherwise does not readily compliment. Secreted split-Gluc fragments were hypothesized to reconstitute functional Gluc in a concentration dependent manner, with higher luciferase activity measured in cultures with cells secreting N-Gluc and C-Gluc respectively in closer proximity to one another.

To validate this, laser cut stencils were fabricated with two chambers, each .32 cm^2 in area, separated by distances of 1, 2, 3, 5, 7, 10, 20, or 30 mm. Cells expressing Jun-NGluc were plated in one chamber, and Fos-CGluc-expressing cells were plated in the other. After 24 h, fresh media was added to cover the surface of each stencil allowed to mix with existing supernatant. Media aliquots were then collected and imaged to produce the data in Figure 2.4.

2.4 DNA-programmed cell patterning

Higher resolution patterns (μm scale) of both contacting and non-contacting cells, such as those used in the previously discussed structured liver co-cultures, can be produced through micropatterning of ECM-proteins which promote cell adhesion [4, 5]. These approaches are generally limited to specifying structured adhesion of a single cell type (with a second cell type potentially used to fill in negative un-patterned areas) because of the lack of cell-type specificity of adhesion to most ECM proteins such as fibronectin or collagen. This limitation can be addressed by employing the base-pairing specificity of complimentary single-stranded

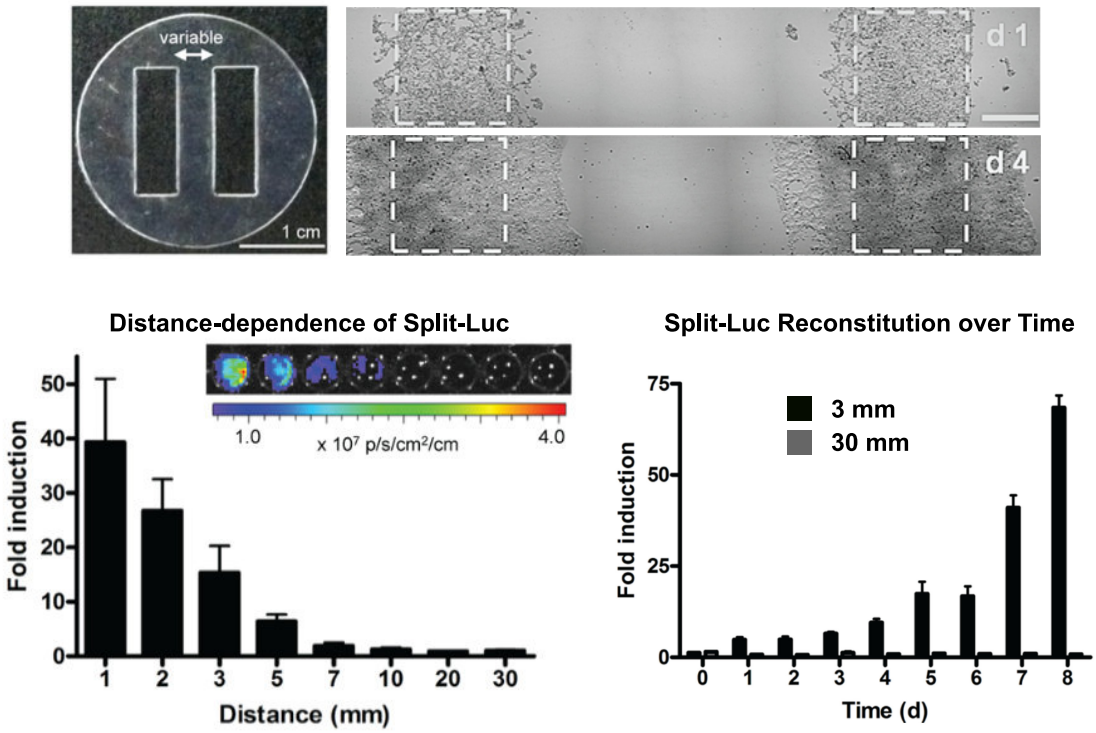

Figure 2.4: Distance Dependent Reconstitution of Secreted Split-Gluc
Top Left: Photograph of laser-cut stencil. Top Right: Example of cells seeded using the stencils, after 1 and 4 days post seeding. Bottom Left: Fold-induction of bioluminescent signals from cells expressing Jun-NGluc and Fos-CGluc plated 1−30 mm apart from Fos-CGluc-expressing cells versus or control cells (expressing CGluc only). Error bars are standard error of the mean from n = 6 replicates. Inset: sample bioluminescence images for the Jun-NGluc/Fos-CGluc pairings at each distance. Bottom Right: Tracking bioluminescence produced over multiple days following stencil removal. Error bars are standard error of the mean for n = 3 replicates.

DNA to program cell adhesion to a surface. Single-stranded DNA oligomers can be immobilized to a target surface via either physical adsorption, electrostatic interaction, or covalent attachment [6, 7]. Similarly, techniques have been developed for decorating the outer surface of both eukaryotic and prokaryotic cells with single-stranded DNA [8]. Cells labeled in such a manner bind preferentially to areas with DNA complimentary to the cell surface. Additional cell types can be simultaneously patterned within the same region by using additional complimentary ssDNA pairs, with independent patterning of as many as 4 distinct cell types demonstrated [9].

The kinetics of DNA-complementation driven attachment is fast [10], allowing multiple cell types to be patterned in quick succession separated only by short 5-10 minutes incubations and washes rather than the hours long pauses which would be necessary to allow integrin-based adhesions to form. This approach has the further advantage of allowing patterning of non-adherent cell types which do not form integrin-based adhesions to ECM proteins.

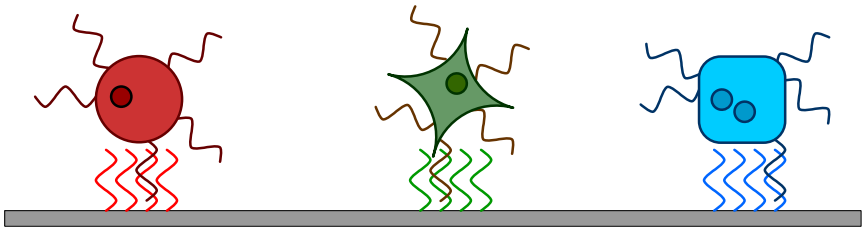

Figure 2.5: Schematic of DNA-progranned cell patterning
Dark and light strands of the same color represent complimentary ssDNA. Cells decorated with ssDNA preferentially adhere to regions of a substrate with immobilized DNA of complementary sequence.

Table 2.1: DNA sequences used for patterning

Oligo name	Sequence
A	ACTGACTGACTGACTGACTG
A'	CAGTCAGTCAGTCAGTCAGT
F	AGAAGAAGAACGAAGAAGAA
F'	TTCTTCTTCGTTCTTCTTCT

2.4.1 DNA immobilization on glass substrate

Thanks in part to the abundance of applications of DNA micro-arrays in biotechnology, many strategies exist for immobilizing single stranded DNA to glass surfaces. We elected to proceed with immobilizing amine-functionalized DNA to aldehyde-coated glass; this chemistry was previously determined to provide the best balance of high immobilization density while being easily adapted across multiple substrate materials using silane surface modifications [7].

While immobilization of ssDNA by simple electrostatic interaction or physical adsorption can successfully support hybridization of target DNA in solution, covalent attachment is preferable for supporting cell attachment to limit detachment of DNA from the substrate surface [11].

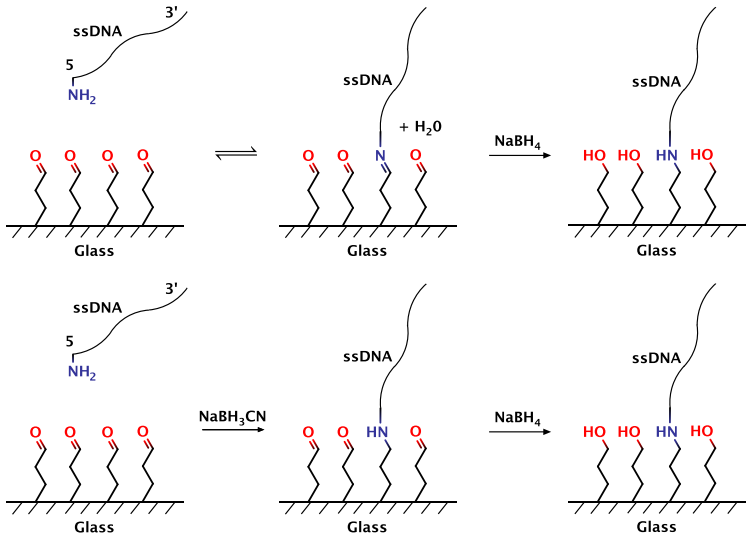

Figure 2.6: Schematic of Amine-Aldehyde Immobilization Chemistry
Top: Original scheme of amine-DNA conjugation to aldehyde-coated glass. Bottom: Modified scheme with mild reducing agent $NaBH_3CN$ included in immobilization buffer.

Covalent attachment of amine-modified DNA to aldehyde-coated glass proceeds in several stages summarized in Figure 2.6. Immobilization buffer composition, pH, and spot-drying have all been found to impact the efficiency and uniformity of DNA immobilization to glass [12]. In solution, terminal amines form a Schiff-base linkage through nucleophilic addition to the carbonyl carbon followed by dehydration to generate a hydrolizable imide bond. The glass slide is then dehydrated in a 120 $^\circ$C oven and the imines are reduced to non-hydrolyzable amides in a solution containing sodium borohydride. Slides are then treated with silane and pluronic to block unwanted cell adhesion in unpatterned areas. A full stepwise protocol is in Section 2.6.3.

Commercial microspotters, commonly used to generate DNA and protein microarrays, can create custom spot arrays for DNA patterning. Purpose-built pins are micro-machined with

capillary channels such that DNA solutions can be loaded and deposited by briefly contacting the pin tip to target substrate. Spot size determined by spotting buffer composition, pin dimensions, and relative humidity during spotting. Single spot delivery volumes can be as low as 600 pL to produce spots less than 50μm in diameter. Through some creative adjustments to commercial microspotter control software, larger connected regions can be formed through overlapping spots.

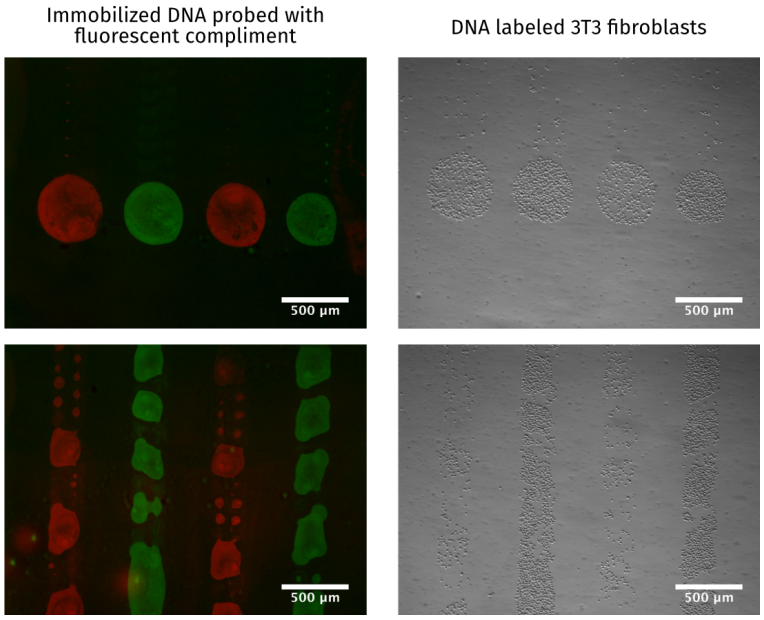

Figure 2.7: DNA patterns generated by Microspotting

We found that successful immobilization with the amine-aldehyde conjugation chemistry requires drying of spotted amine-DNA solution on the surface of the glass substrate (Fig. 2.8). This matches reports in literature [13], which suggest the reason as a combination of the concentrating effect on amine-DNA as solution volume decreases and the removal of water preventing the reverse imide hydroloysis reaction. This was found to be problematic for producing larger (>500 μm) continuous areas of immobilized DNA as uneven drying lead to non-uniform immobilization (as in Figs. 2.7 and 2.9). We were able to circumvent these issues and eliminate the need to a drying step by modifying the immobilization buffer to include sodium cyanoborohydride as a mild reducing agent. This allows reductive amination of the amine-aldehyde conjugation to proceed to form the non-hydrolyzable amide bond in

the patterning solution. Importantly, the less aggressive sodium cyanoborohydride is unable to reduce aldehydes to alcohols, which ensures amine-DNA is able to react fully [14]. Later processing steps still include reduction in sodium borohydride to reduce unreacted aldehydes and prevent unwanted conjugation of other amine-containing contaminants.

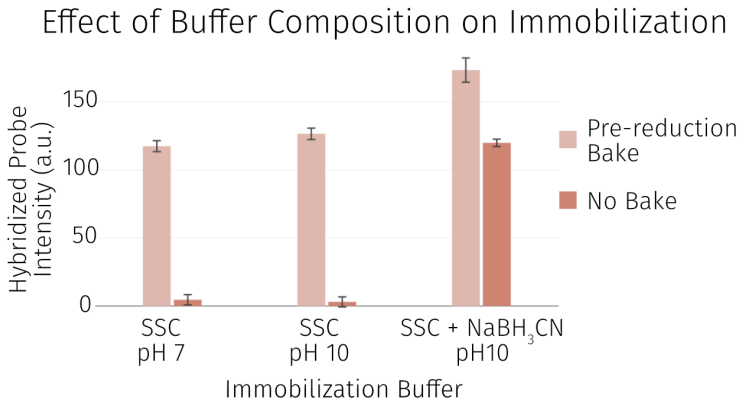

Figure 2.8: Effect of buffer composition and dehydration bake on DNA immobilization Amine-DNA resuspended in specified buffers at 1 mM and incubated in a .5 μL drop on aldehyde-glass for 16 hours. Spots are probed with 125 nM of FITC-labeled complimentary ssDNA and imaged with epifluorescnece on an inverted microscope. Error bars are standard deviation of intensities measured from 3 individual drops.

Microfluidic DNA patterning

Though commercial microspotter and direct printing instruments offer a variety of geometries through a range of different print head sizes producing spots from tens to hundreds of microns in diameter, they are intended for the production of rectangular arrays of spots; larger connected regions must be formed through overlapping spots. The serial nature of the printing process, typically maxing out at around 3000 spots/hour, also becomes limiting for larger pattern areas such as might be needed to produce in vitro co-culture models for high-throughput or high-content screening.

We sought to demonstrate feasibility of using microfluidic channels to pattern immobilized ssDNA in large connected regions. This approach has previously been shown to be effective in patterning amine-modified ssDNA to both glass and plastics coated with NHS-ester

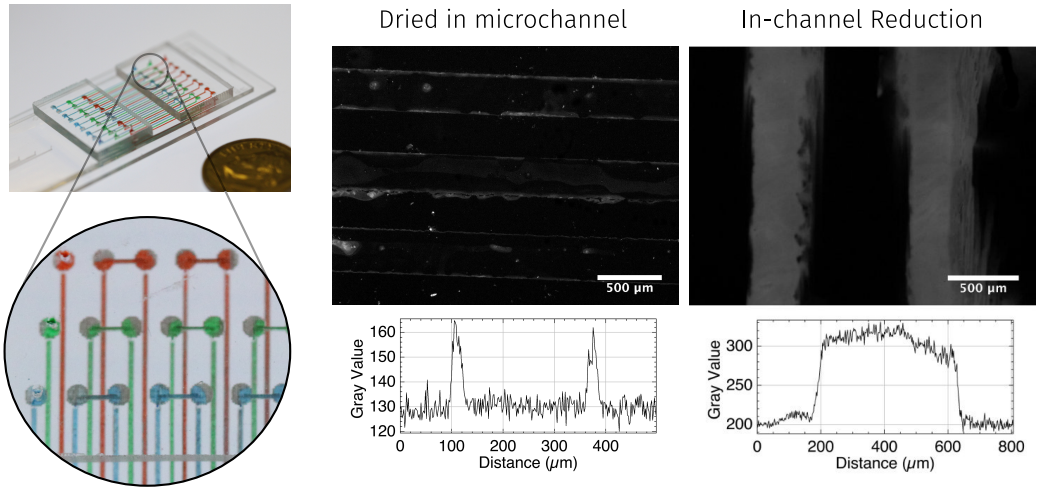

Figure 2.9: Microfluidic Immobilization of Amine-DNA
Left: Laser-cut two-layer microfluidic device for patterning in channels. Inset shows detail of flow channels open to the target glass substrate (vertical channels) connecting with vias to manifold channels in a layer above (horizontal channels). Middle and right: Immobilized DNA patterns produced in microchannels using original scheme or with modified immobilization buffer with reducing agent, probed with fluorescent compliment. Fluorescence intensity profiles are drawn across one representatitve channel.

functional groups [15, 16]. However the density of immobilized DNA in these previous applications, intended for use in hybridization detection of free nucleic acids, is 2-3 orders of magnitude lower than necessary for DNA-programmed cell adhesion. By using a two layer device such as in Figure 2.9, open channels directly interfacing the target glass substrate can be connected by vias to a second manifold layer, eliminating the need to balance flow impedance across channels for different DNA solutions. This enables the parallel creation of large areas of immobilized DNA.

2.4.2 Incorporation of DNA into cell plasma membranes

As with immobilization of DNA to glass surfaces, multiple strategies exist for the decoration of extracellular surfaces with ssDNA, many stemming from work in the lab of Carolyn Bertozzi. These include modification of one termini of ssDNA with a chemical conjugation handle targeting either sialic acid-containing glycoproteins [10] or exposed peptide amines

[11]. Lipid-DNA conjugates can also be used, allowing direct insertion of ssDNA covalently linked at the 5' end to a 20-carbon dialkylglycerol group into the extracellular plasma membrane [17]. The lifetime and maximum density of DNA incorporated in this manner are both improved by the addition of a second 3' lipid-conjugated ssDNA "co-anchor" strand. [18] The anchor and co-anchor strand share 20nt of complementation at their 5' and 3' ends, respectively. The anchor strand further includes a 60nt poly-thymine spacer followed by a 20nt pattern specific region.

The passive physical insertion of lipid-conjugated DNA has been found to work efficiently across many cell types, and as it does not require prior chemical or genetic modification of the target cells, is also amenable to labeling primary cells. We quantified the incorporation efficiency and specificity of lipid-DNA into two fibroblast cell lines (NIH and Swiss 3T3s), and epithelial cell line (NMUMG), and a liver cancer cell line (HepG2) using a flow cytometry assay outlined in Section 2.6.5. Across all cell lines tested, successful incorporation of A' or F' DNA was found in $>70\%$ of cells, with $<5\%$ of cells picking up nonspecific hybridization of non complimentary probe DNA.

2.4.3 Fidelity of DNA-programmed cell patterning

To evaluate quality of heterotypic cell patterns achieved through DNA-programmed adhesion, we used flow cells to seed A' and F' labeled NIH 3T3 fibroblasts onto slides with A and F immobilized DNA manually spotted by pipette. "On-target" rate describes the fraction of a given cell type which seeds to the correctly coded immobilized DNA spot, while "Cross-contamination" measures the extent to which DNA spots harbor attachment by cells with non-complimentary anchor strands. Sample equations for these calculations applied to A-adhesion strand coded spots are given in Eqs. 2.1 and 2.2.

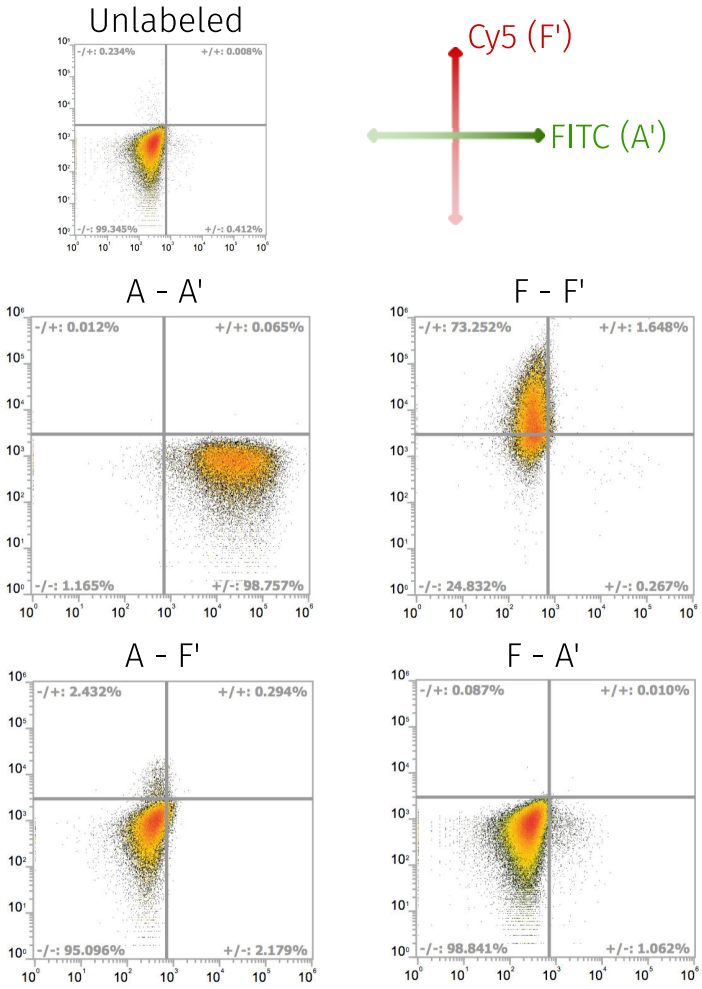

Figure 2.10: Quantifying lipid-DNA incorporation by flow cytometry
Unlabeled: NIH 3T3s with no Lipid-DNA and no probe DNA. A-A': A-adhesion DNA labeled NIH 3T3s probed with FITC-labeled A' DNA. F-F': F-adhesion DNA labeled NIH 3T3s probed with Cy5-labeled F' DNA. A-F': A-adhesion DNA labeled NIH 3T3s probed with Cy5-labeled F' DNA. F-A': F-adhesion DNA labeled NIH 3T3s probed with FITC-labeled A' DNA. X and Y axis are log-FITC and log-Cy5 signal, respectively.

$$\text{On-Target}_A = \frac{A_{\text{on spot}}}{A_{\text{on spot}} + A_{\text{off spot}}} \tag{2.1}$$

$$\text{Cross-Contamination}_A = \frac{F_{\text{on spot}}}{A_{\text{on spot}} + F_{\text{on spot}}} \tag{2.2}$$

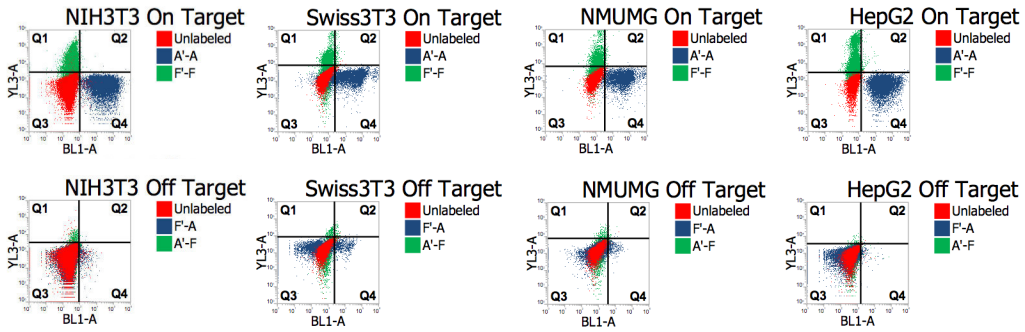

Figure 2.11: Summary of lipid-DNA incorporation across cell types
Two fibroblast lines (NIH 3T3 and Swiss 3T3), epithelial cells (NMUMG), and liver cancer line (HepG2)

Table 2.2: Summary of DNA-patterned co-culture fidelity

Immobilized DNA	On Target	Cross-Contamination
A	$95.5\% \pm 1.7$	$10.6\% \pm 3.5$
F	$95.2\% \pm 2.2$	$2.1\% \pm 1.1$

2.5 Conclusion

We demonstrated various cell patterning methods, each designed to improve a specific experimental parameter. For patterning mm-scale patterns, useful in studying longer-range paracrine signaling, we employed simple laser-cut stencils. Importantly, this approach allows rapid redesign turnaround, allowing patterned geometries to be quickly return in response to preliminary experimental data. For contacting interfaces, we designed a reconfigrable elastic substrate, leveraging the self-healing properties of PDMS to form a clean interface between two cell types after seeding independently on two sides of a removable barrier. And finally, towards extending patterning beyond 2 cell types, we adopted DNA-patterned adhesion, optimizing functionalization chemistry to enable parallel immobilization of ssDNA patterns over large areas using microfluidic patterning.

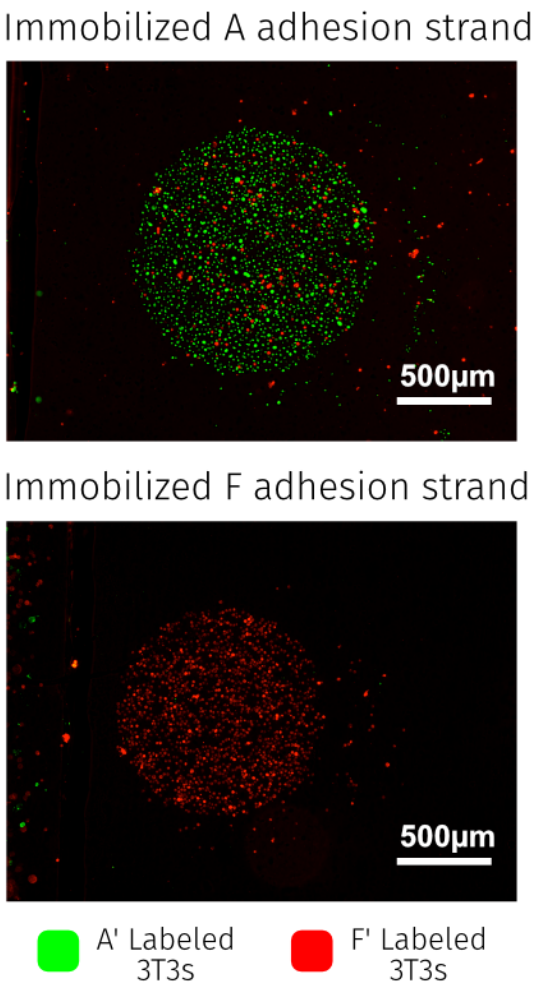

Figure 2.12: DNA-programmed heterotypic cell pattern

This third a in particular enables several interesting experiments. First, we are interested in applying DNA-patterning to produce structured hepatocyte co-cultures with additional liver-associated cell types included in addition to the current standard stromal fibroblasts. For screening drug-induced liver damage, we anticipate increasing the number of cell types included in these *in vitro* models can improve their physiological relevance and produce better predictions of liver responses *in vivo*. While current DNA patterning experiments are seeded in a flow-cell which is removed once co-cultures are established, future experiments could be performed with an intact flow cell. Existing hepatocyte-fibroblast co-cultures have not found to exhibit improve physiological relevance with flow, but this could change as other cell

types such as endothelial cells and macrophages are added. Culture in flow chambers is also attractive for ADME and PK-PD studies to allow easy retrieval and analysis of metabolites [19].

Finally, a number of the patterning tools described in this chapter can be useful in tissue culture models of morphogen gradient patterned development. Investigations traditionally done in invertebrate models *in vivo* can benefit from "bottom up" *in vitro* models in which morphogen response pathways can be more easily rewired and studied in isolation from other interfering pathways [20]. Conflicting models of patterning by secreted Hedgehog proteins, for example, have not resolved the extent to which Hedgehog transport is dependent interaction with sulfated proteoglycans and its principle receptor Patched. Full knockdown of either component completely eliminates Hedgehog mediated responses, but by enabling patterning of a non-uniform field of receiver cells with independent control over modifications to their expressed suface glycoproteins or Hedgehog receptors, DNA-programmed patterning could help to identify the extent to which each contribute to Hedgehog transport. Changes to intracellular signal transduction circuitry interpreting Hedgehog binding which are hypothesized to extend or shorten gradient length can also be confirmed by patterning modified and unmodified receivers in one field.

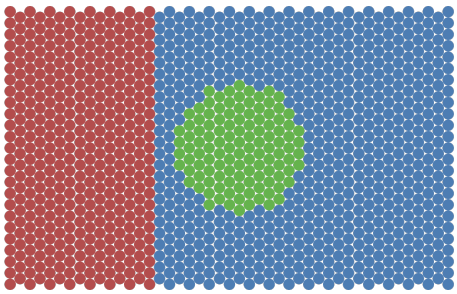

Figure 2.13: Example 3-cell pattern to confirm changes which alter morphogen gradient length/speed

2.6 Methods

2.6.1 Cell patterning with laser-cut stencils

Stencil Fabrication

1. Draw desired features using AutoCAD software (Autodesk, USA).
2. Cut pre-cast 250μm-thick PDMS sheets (HT-6240, Rogers Corp, USA) using a VLS 2.30 30W CO_2 laser (Universal Laser Systems, Scottsdale, AZ) at 50% power and 10% speed.
3. Rinse stencils in 70% ethanol and adhere to tissue culture treated plastic ware.

Cell Seeding

1. Seed cells at high density (1-3 x 10^5 cells/cm^2 and allow to adhere for 24 hours.
2. Remove and peel stencil away carefully.
3. Add appropriate amount of fresh cell culture media for well size used.

2.6.2 Fabricating reconfigurable elastomeric substrates for patterning clean boundaries

Device Fabrication

1. Generate a mold by adhering laser cut acrylic pieces (20mm circles, 6mm thick) to the base of a shallow, flat dish using cyanoacrylate glue (Gorilla Glue Company, USA).

2. Prepare PDMS at a 10:1 ratio of base to curing agent (Sylgard 184, Dow Corning, USA), degas in a vacuum chamber, and pour the degassed mixture atop the mold. Allow the mixture to cure at 65 $^{\circ}$C for 4 hours.

3. Remove the mold and cut the PDMS into individual devices (50mm x 25mm x 8.25mm)

4. Mount a razor blade into the cutting rig shown in Figure 2.3 and cut slices through the center of the device well.

5. Sterilize the device prior to use in cell culture experiments by placing under UV irradiation overnight or rinsing and drying in 70% ethanol.

Cell Seeding

1. UV-sterilized overnight and treated for 60 seconds with a plasma formed from room air.

2. Coat device wells with ECM protein for cell adhesion by incubating with 200 mL of 5 mg/mL human fibronectin (Sigma-Aldrich, USA) at room temperature (RT) for 3 hours, then rinsing once with 200-400 mL sterile PBS.

3. Open the device slit by bending the device, and insert a glass coverslip (#1, Fisher-Scientific, USA) to seal each well half.

4. Seed each side with cells. Number and duration of seeding will vary depending on cell type and size; for images in Figure 2.1, two 3T3 cell lines expressing H2b-mTurquoise and H2b-Citrine respectively were each seeded at 0.5 x 10^6 in 500 mL media and allowed to adhere for 3–5 hours.

5. Unadhered cells are aspirated away and the well washed three times with warm PBS.

6. Bend the device gently and remove the coverslip, then allow the slit to reseal and wash another three times with warm PBS.

7. Fill the well with 1 mL of appropriate cell culture media.

2.6.3 Preparation of DNA-patterned glass slides

The following protocols are adapted from [21].

Microspotter Patterning

1. Resuspend each amine-modified anchor DNA at 1mM in freshly prepared Spotting Buffer (3x SSC, pH 10, with 0.4 mg/ml n-octylglucoside).

2. Spot desired patterns using a commercial microspotter, following instrument-specific procedures. Spot size and uniformity was found to be best when printing in 65% relative humidity.

3. Dehydrate patterned slide in 120 $^\circ$C oven for 15-30 minutes. Slides can then be finished by proceeding through the steps in "Post Patterning Treatments", or stored in a vacuum desiccator for up to a month.

Microfluidic Patterning

1. Form 2mm and 5mm thick slabs of PDMS for use as flow and manifold layers by pouring 10 and 30 g of degassed PDMS prepolymer mixed at 10:1 base:crosslinker into 100mm square petri dishes (Thermo-Fisher).

2. Cure slabs for 2 hours at 65 $^\circ$C.

3. Using a VLS 2.30 30W CO_2 laser (Universal Laser Systems, Scottsdale, AZ), cut channels and through-holes in flow and manifold layers. See Table 2.3 for laser cut settings. 500 μm wide channels are formed as 5 parallel cuts spaced 50 μm apart.

Table 2.3: VersaLaser Settings for Microfluidic DNA Patterning Devices

Feature Type	**Power**	**Speed**	**PPI**
Lettering	15	100	1000
Flow Layer Channels	.8	1.8	1000
Manifold Layer Channels	.8	1.8	1000
Vias/Thru-cuts (2 mm PDMS)	80	15	1000
Vias/Thru-cuts (5 mm PDMS)	80	5	1000

4. Clean laser-cut pieces by first rinsing in 70% EtOH, then sonicating for 5 minutes in IPA and twice for 5-10 minutes in water. Dry under clean nitrogen stream.

5. Plasma activate both flow layer and manifold layer pieces in Harrick O_2 Plasma Cleaner at for 2 minutes at 200 mTorr on high RF power, and immediately align and press the two pieces together to form a permanent bond.

6. Place assembled microfluidic on top of aldehyde-coated glass slide (Schott Nexterion). Press gently to form a tight but reversible seal.

7. Resuspend each amine-modified anchor DNA at 1mM in freshly prepared Immobilization Buffer (3x SSC, pH 10, with 50 μM $NaBH_3CN$).

8. Pipette a small volume (1-5 μL) of amine-DNA solution at channel inlets. If the microfluidic channels were properly plasma activated, capillary action will quickly pull solution through up to several cm of channel length. Longer channels can be filled by adding a larger volume at the inlet and drawing gentle negative pressure with a Hamilton syringe (1mL) at the outlet.

9. Incubate loaded microfluidic device in 100% relative humidity for 12-16 hours.

10. Place entire assembly into a crystallizing dish filled with enough .1% SDS to completely submerge the device, and quickly peel the microfluidic layers off the glass slide using tweezers.

11. Aspirate the .1% SDS and rinse twice in distilled water, agitating gently. Slides can then be finished by proceeding through the steps in "Post Patterning Treatments", or stored in a vacuum desiccator for up to a month.

Post-patterning Treatments

After anchor-strand DNA has been immobilized on the surface, slides are treated in $NaBH_4$ to reduce unreacted aldehydes, then passivated with silane and pluronic to block unwanted cell adhesion in empty regions.

1. Place up to four slides into a 150mm glass crystallizing dish, and cover with 50 mL freshly prepared $NaBH_4$ solution (12.5 mL pure ethanol, 37.5 mL PBS, 125 mg $NaBH_4$). Incubate for 15 minutes shaking at 120 rpm on an orbital shaker.

2. Aspirate and dispose of $NaBH_4$ solution.

3. In the same dish, immerse the slides in 0.1% SDS in PBS. Agitate 10 times then dispose of the wash. Repeat once.

4. In the same dish, immerse the slides in distilled water. Agitate 10 times then dispose of the wash. Repeat twice.

5. Prepare a solution of 10% acetic acid in water in a 50-ml conical tube. Place one patterned slide at a time in the tube, cap, and invert 20 times. Remove the slide from the tube with tweezers and dry under an air or nitrogen nozzle.

6. Using glass transferware, combine 60 ml dichloromethane, 600 μl tridecafluoro-1,1,2,2-tetrahydrooctyl)dimethylchlorosilane, and 600 μl triethylamine in a glass Coplin jar.

7. Place u to 4 patterned slides in the Coplin jar and shake at 120 rpm for 15 min on an orbital shaker.

8. Fill two 50mL connical tubes with dichloromethane, a third with absolute ethanol, and a fourth with distilled water.

9. Working with tweezers, transfer one slide at a time into the first conical tube, cap, and invert ten times. Repeat in each of the four conical in sequence to wash. Dry slides at the end under a stream of clean nitrogen.

2.6.4 Incorporation of Lipid-DNA into cell membranes

Lipid DNA generously provided by Katie Cabral from Zev Gartner's lab at UCSF; the following protocol is adapted from [21].

1. Prepare a suspension of cells to be labeled and wash three times in ice-cold sterile 1x calcium and magnesium-free PBS. Perform all following steps at 4 $^\circ$ C to minimize cell death.

2. Resuspend cells at 2 x 10^7 cells/mL in PBS.

3. Add 1 μl of the 50 μM adhesion strand solution to the cell suspension, mix thoroughly by pipetting, and incubate for 10 minutes on ice.

4. Add 1 μl of the 50 μM co-anchor strand solution to the cell suspension, mix thoroughly by pipetting, and incubate for 10 minutes on ice.

5. Wash three times in PBS to remove excess lipid-DNA.

6. Resuspend in 50-100 μL Flow Buffer

2.6.5 Quantifying Lipid-DNA incorporation by flow cytometry

1. Suspend 9 x 10^6 cells, and follow the protocol laid out in 2.6.4 to label 3 x 10^6 cells each with A' adhesion strands, F' adhesion strands, and PBS containing no lipid-DNA as a negative control.
2. Split each of the above into three separate tubes (reulting in 9 total tubes).
3. Add 1 μL of 125 nM FITC-labeled A DNA (Genewiz, South Plainfield, NJ) into the first tube.
4. Add 1 μL of 125 nM Cy5-labeled F DNA (Genewiz, South Plainfield, NJ) into the second tube.
5. Add 1 uL of PBS in the third tube.
6. Incubate tubes, shielded from light at room temperature, for 30 minutes.
7. Wash tubes three times with PBS. Resuspend each tube in 300-500 μL PBS and run on flow cytometer to measure Cy5 and FITC signal.

2.6.6 DNA-patterned Cell Seeding

1. Construct simple flow cells by molding PDMS around 8mm x 20mm x 200μm thick piece of mylar plastic (alternatively, a 22x22 #1 glass coverslip nroken in half).
2. Plasma treat flow cells (to make surfaces hydrophilic and promote even flow) in a Harrick O2 Plasma Cleaner for 30 seconds - 2 minutes at 200mTorr at high power.
3. Mount flow cells over DNA patterns produced on glass slides by procedure 2.6.3, pressing gently to form a tight but reversible seal.

4. Prime flow cells with priming buffer (.1 g MgCl2, .1 g CaCl2, 100 uL Tween-20, 99.325 mL MilliQ Water, 575 uL Glacial Acetic Acid).

5. Suspend cells and follow protocol 2.6.4 to label with appropriate lipid-DNA.

6. Resuspend labeled cells at 2-4 x10^7 per mL in Flow Buffer (2 g BSA, .5 g EDTA disodium dihydrate, 1 g Pluronic F68, 99 mL PBS). Keep cell suspensions as close to 4 $^\circ$ C as possible through all following steps.

7. For each cell type to be patterned: Flush each flow cell with 100-250 μL of Flow Buffer. Angle the flow cell to allow gravity to drive flow from inlet to outlet. Flow in 20-50 μL of lipid-DNA labeled cells. Flush by recycling flow-through at bottom of flow cell and reintroducing it at the inlet; repeat 10-20 times. Incubate cell-laden flow cell on a level surface at 4 $^\circ$ C for 5-10 minutes. Flush flow cell with 100-250 μL of Flow Buffer to clear unattached cells.

8. After seeding all cell types, carefully remove flow cells with tweezers and cover slide in appropriate cell growth media and place covered in cell culture incubator.

Bibliography

[1] S. R. Khetani and S. N. Bhatia, "Microscale culture of human liver cells for drug development.," *Nature biotechnology*, vol. 26, pp. 120–6, jan 2008.

[2] E. E. Hui and S. N. Bhatia, "Microscale Control of Cell Contact and Spacing via Three-Component Surface Patterning," *Langmuir*, vol. 23, pp. 4103–4107, apr 2007.

[3] E. Ostuni, R. Kane, C. S. Chen, D. E. Ingber, and G. M. Whitesides, "Patterning mammalian cells using elastomeric membranes," *Langmuir*, vol. 16, no. 20, pp. 7811–7819, 2000.

[4] R. Singhvi, A. Kumar, G. Lopez, G. Stephanopoulos, D. Wang, G. Whitesides, and D. Ingber, "Engineering cell shape and function," *Science*, vol. 264, pp. 696–698, apr 1994.

[5] J. L. Tan, W. Liu, C. M. Nelson, S. Raghavan, and C. S. Chen, "Simple Approach to Micropattern Cells on Common Culture Substrates by Tuning Substrate Wettability," *Tissue Engineering*, vol. 10, pp. 865–872, may 2004.

[6] S. Taylor, "Impact of surface chemistry and blocking strategies on DNA microarrays," *Nucleic Acids Research*, vol. 31, pp. 87e–87, aug 2003.

[7] N. Zammatteo, L. Jeanmart, S. Hamels, S. Courtois, P. Louette, L. Hevesi, and J. Remacle, "Comparison between Different Strategies of Covalent Attachment of DNA to Glass Surfaces to Build DNA Microarrays," *Analytical Biochemistry*, vol. 280, pp. 143–150, apr 2000.

[8] J. S. Liu and Z. J. Gartner, "Directing the assembly of spatially organized multicomponent tissues from the bottom up," 2012.

[9] S. Chen, A. W. Bremer, O. J. Scheideler, Y. S. Na, M. E. Todhunter, S. Hsiao, P. R. Bomdica, M. M. Maharbiz, Z. J. Gartner, and D. V. Schaffer, "Interrogating cellular fate decisions with high-throughput arrays of multiplexed cellular communities," *Nature Communications*, vol. 7, p. 10309, jan 2016.

[10] Z. J. Gartner and C. R. Bertozzi, "Programmed assembly of 3-dimensional microtissues with defined cellular connectivity," *Proceedings of the National Academy of Sciences*, vol. 106, no. 12, pp. 4606–4610, 2009.

[11] S. C. Hsiao, B. J. Shum, H. Onoe, E. S. Douglas, Z. J. Gartner, R. A. Mathies, C. R. Bertozzi, and M. B. Francis, "Direct Cell Surface Modification with DNA for the Capture of Primary Cells and the Investigation of Myotube Formation on Defined Patterns," *Langmuir*, vol. 25, pp. 6985–6991, jun 2009.

[12] E. D. Dawson, A. E. Reppert, K. L. Rowlen, and L. R. Kuck, "Spotting optimization for oligo microarrays on aldehyde–glass," *Analytical Biochemistry*, vol. 341, pp. 352–360, jun 2005.

[13] J. Sobek, C. Aquino, W. Weigel, and R. Schlapbach, "Drop drying on surfaces determines chemical reactivity - the specific case of immobilization of oligonucleotides on microarrays.," *BMC biophysics*, vol. 6, no. 1, p. 8, 2013.

[14] J. M. Goddard and D. Erickson, "Bioconjugation techniques for microfluidic biosensors," *Analytical and Bioanalytical Chemistry*, vol. 394, pp. 469–479, may 2009.

[15] M. Geissler, E. Roy, G. A. Diaz-Quijada, J.-C. C. Galas, and T. Veres, "Microfluidic Patterning of Miniaturized DNA Arrays on Plastic Substrates," *ACS Applied Materials and Interfaces*, vol. 1, pp. 1387–1395, jul 2009.

[16] D. Brassard, L. Clime, K. Li, M. Geissler, C. Miville-Godin, E. Roy, and T. Veres, "3D thermoplastic elastomer microfluidic devices for biological probe immobilization," *Lab on a Chip*, vol. 11, no. 23, p. 4099, 2011.

[17] N. S. Selden, M. E. Todhunter, N. Y. Jee, J. S. Liu, K. E. Broaders, and Z. J. Gartner, "Chemically Programmed Cell Adhesion with Membrane-Anchored Oligonucleotides," *Journal of the American Chemical Society*, vol. 134, pp. 765–768, jan 2012.

[18] R. J. Weber, S. I. Liang, N. S. Selden, T. A. Desai, and Z. J. Gartner, "Efficient targeting of fatty-acid modified oligonucleotides to live cell membranes through stepwise assembly," *Biomacromolecules*, vol. 15, pp. 4621–4626, dec 2014.

[19] E. Novik, T. J. Maguire, P. Chao, K. C. Cheng, and M. L. Yarmush, "A microfluidic hepatic coculture platform for cell-based drug metabolism studies," *Biochemical Pharmacology*, vol. 79, pp. 1036–1044, apr 2010.

[20] P. Li, J. S. Markson, S. Wang, S. Chen, V. Vachharajani, and M. B. Elowitz, "Morphogen gradient reconstitution reveals Hedgehog pathway design principles," *Science*, vol. 360, pp. 543–548, may 2018.

[21] M. E. Todhunter, R. J. Weber, J. Farlow, N. Y. Jee, A. E. Cerchiari, and Z. J. Gartner, "Fabrication of 3-D Reconstituted Organoid Arrays by DNA-Programmed Assembly of Cells (DPAC)," in *Current Protocols in Chemical Biology*, pp. 147–178, Hoboken, NJ, USA: John Wiley & Sons, Inc., sep 2016.

Chapter 3

Engineering light-activated gene expression in yeast

3.1 Introduction

Standard cell biology manipulations such as the use of gene knockouts or small molecule inhibitors have allowed researchers to define the contribution of a tremendous number of cellular components to specific biological processes. However, the lack of methods for precise, dynamic inputs limited cell biologists' ability to study the dynamics of the interacting protein networks which are responsible for many cell behaviors. The field of optogenetics seeks to address these challenges by using light as a controlled input to perturb key cellular components, leveraging the ease with which optical signals can be both spatially and temporally presented. While the first demonstrations of light-based cellular perturbation used light-gated ion-channels to control the membrane potential of neurons, other light-sensitive systems have been engineered to control protein structure, localization, and binding inter-

action, broadening the reach of optical manipulation to a wide range of cellular signaling transduction events [1].

Dynamic cellular responses are commonly read out by live imaging genetically encoded fluorescent protein reporters such as GFP. The wide range of fluorescent proteins available at different wavelengths of excitation and emission allows multiple components of interest to be simultaneously and independently recorded. Multiple channels of dynamic control could be similarly achieved through mutually orthogonal optogenetic controllers which are sensitive to distinct light inputs. In addition to expanding the number of cell states that can be programmed in schemes employing optogentic control of gene expression, this is also attractive towards elucidating protein network dynamics. In networks where cross-talk exists between pathways, optogenetic control of multiple independent nodes in the network can help in providing isolation and controlled perturbation of only one pathway.

In this chapter we present work towards multichannel optogenetics using the photoswitchable protein-protein interaction of arabidopsis proteins Phytochrome B (PhyB) and Phytochrome Interacting Factor (PIF). Working in yeast two-hybrid platform to tie PhyB-PIF association to expression of reporter genes, we pursued two strategies to engineer the light-responsive behavior of light-activated gene expression. First, we sought to establish a platform for genetic selection of PhyB variants with desired photoactivity from large libraries of mutants. We targeted this platform towards indentification of spectral variants which would exhibit photoswitched interaction to PIF at wavelengths of light distinct from the wild type. Second, we hypothesized that the response speed of PhyB-PIF driven gene expression could also be engineered to produce faster or slower responding pairs by altering the subcellular localization of the two components. Success in this approach could allow multiplexing optogenetic control through tuning light excitation duration rather than wavelength.

3.2 Background

3.2.1 Optogenetic Tools for Controlling Protein-Protein Interactions

Optical control of protein-protein interactions has been achieved in a number of ways. Commonly, these methods rely on a photosensitive protein which undergoes a conformational change in response to specific light excitation, producing a change in its binding affinity for a interacting partner. The most successful variants of this approach are summarized in Table 3.1. Additional systems using photocaged chemical dimerizers [2] or a light-sensitive unnatural amino acids [3] are also promising. The irreversibility of photocaged systems limit their usefulness as dynamic system inputs, however. While incorporation of an unnatural amino acid which photoisomerizes and drives changes in structure and function of the larger protein is an attractive and potentially very powerful strategy, to date it has lacked the ease of modular design, requiring non-trivial engineering to adapt for a new target protein.

A key advantage of the Phy/PIF system over other optogenetic controllers is the fast, photoreversible nature of its interaction. Many other optically inducible protein-protein interactions are reversible only through slow thermal reversion to the dark state. Dronpa dimerization is closest to matching Phy/PIF in binding/unbinding kinetics, and the innate fluorescence of the Dronpa protein itself can simplify experimental schemes for live, simultaneous optical perturbation and imaging. However the homodimerizing nature of Dronpa limits its use in schemes in which heterotypic interaction between two different proteins of interest is desired.

Table 3.1: Optogenetic Systems for Controlling Protein-Protein Interactions

	Developed By	Interaction Type	Reversible?
CRY2-CIB1	Kennedy et al, 2010 [4]	Heterodimer	Yes (slow)
CRY2	Bugaj et al, 2013 [5]	Oligomer	Yes (slow)
Dronpa	Zhou et al, 2012 [6]	Dimer/Tetramer	Yes (fast)
Gigantea-FKF1	Yazawa et al, 2009 [7]	Heterodimer	No
Phy-PIF	Levskaya et al, 2009 [8]	Heterodimer	Yes (fast)

Existing Multichromatic Optogenetic Technologies

The first demonstration of multichromatic optogenetic control used phytochrome Cph1 and cyanobacteriochrome CcasS/R expressed in E. coli. Both Cph1 and CcasS/R activate gene expression through histidine kinase domains with autophosphorylation and phosphotransfer activities; Cph1 activates under red light and CcasS/R under green. The output of each was to drive the expression of β-galactosidase, producing patterned pigment production when light, specified independently by two color channels of excitation [9].

Similarly, multichromatic control of gene expression was demonstrated in mammalian cells using the combination of PhyB-PIF, VVD, and UVR8 light-responsive proteins, activating under red, blue, and UVB excitation respectively. Each controller is adapted for use as an activator of gene expression by the fusion of a split transcription factor, using localization to a promoter element to initiate transcription [10]. The responses produced by this method, as well as the histidine kinase effector domains of the bacterial system, are sufficient for driving gene expression but are too slow for real-time control of faster cellular processes such as cytoskeletal reorganization. To date, there has not been a demonstration of simultaneous independent control of these dynamic processes.

3.2.2 Phytochrome Photobiology

Phytochrome B (PhyB) acts as a red/far-red light sensor, and switches between conformations with high binding affinity for Phytochrome Interacting Factor (PIF) when exposed to red light (650nm) and a low affinity conformation in far-red light (750nm). This property was first leveraged to adapt PhyB and PIF as an optogenetic controller in mammalian cells in 2009, driving membrane localization of target proteins [8]. By anchoring PhyB to the cell membrane, proteins fused to cytoplasmic PIF are be retained at the membrane by the PhyB-PIF interaction under red light, but released and return to diffuse freely in the cytoplasm when irradiated with far-red light. The fast binding-on and -off kinetics, as well as the reversible nature of the interaction, allowed fine spatial temporal control of protein recruitment, demonstrated functionally by the localization of RhoA-GEFs to induce cytoskeletal contractions exclusively at regions of the cell membrane irradiated with a red laser pointer. Patterned optogenetic control at this subcellular scale cannot be achieved in other systems which do not exhibit photoreversibility, because photoactivated elements which diffuse out of the region under patterned light excitation remain active and blur the effective spatial input pattern.

Molecular basis for light-switchable PhyB binding interaction to PIF

Phytochrome B (PhyB) is a member of the plant phytochromes and features domain organization common within the family: A short unstructured N-terminal stretch followed by a PAS domain, a chromophore-binding GAF domain, a PHY domain, two tandem PAS domains, and finally a C-terminal Histidine Kinase effector domain.

The PAS, GAF and PHY domains together comprise the photosensory core (or PSM, photosensory module) of the protein, and truncated forms of the protein with the last two PAS domains and effector domains removed still exhibit photoswitchable interaction with the

PIF partner [11]. The truncated PSM is also useful for crystallographic studies where the flexbility of the larger native protein is problematic; a protein structure of PhyB from A. thaliana was reported in 2014 [12].

Phytochrome photoswitching behavior is a product of the bilin chromophore bound to the protein in a pocket of the GAF domain. In plants, this chromophore is usually Phytochromobilin (PϕB), though Phycocyanobilin (PCB) can also be incorporated and has the practical advantage of being easily extracted in experimentally practical quantities from commerically available spirulina. In the absence of light, each adopts a Z-enatiomeric form at the carbon 15-16 bond, and absorbs strongly at roughly 650nm due to the long pi conjugated system. Excitation with red light then causes a transisomerization at C15-16 to the 15E isomer, which has a red-shifted absorbance spectra. Excitation with far-red at 750nm photoisomerizes the 15E isomer back to the 15Z form.

A crystal structure of the PhyB photosensory module was recently published [12]. PhyB forms a photoadduct with PCB by a covalent linkage between cysteine 357 in the GAF domain and C3 of the chromophore [13]. The binding pocket of the protein is tight around rings A-C, but the D-ring of the bilin is left relatively free, allowing it to turn through the rotation generated by photoisomerization. A number of residues in the chromophore binding pocket of PhyB, chiefly M274, Y276, Y303, and M365, surround and shield the hydrophobic D ring from solvent in the 15E state. These residues are thought to track with the transisomerization of the chromophore with light, resulting in large-scale conformational changes in PhyB which modulate its binding affinity to PIF.

3.2.3 Phytochrome Family Proteins with Alternative Absorption Spectra

Phytochromes with photocycles sensitive to wavelengths differing from the usual red/far-red have been identified in cyanobacteria and algae [14]. Many of these phytochromes incorporate a bilin chromophore which naturally isomerizes around a different pair of light wavelengths, or differ in the manner by which the bilin is bound within the chromophore pocket. Understanding the mechanisms behind these shifted photocycles is valuable for predicting changes which could effect similar shifts in PhyB's photoswitching behavior.

Cyanobacterial DXCF-motif Cyanobacteriochromes

Cyanobacteriochromes (CBCRs) are phytochrome family proteins found in cyanobacteria, and generally incorporate Phycoviolobilin (PVB) instead of PCB as a chromophore. PVB exhibits similar absorption spectra and photoisomerization behavior to PCB. Early CBCRs such as Cph1 were found to exhibit red/far-red photocycles like plant phytochromes, and featured a similar covalent bond between a cysteine residue in the GAF domain to C3 of the bilin [15]. Strikingly, a subset of CBCRs photoswitch instead around a blue/green cycle despite still PVB as the bilin chromophore. Members of this group have all been found to share a common Asp-Xaa-Cys-Phe (DXCF) motif in the GAF domain not seen in other phytochromes. The cysteine residue in this motif forms a second covalent linkage to the bilin chromophore at C10 [13]. This bond breaks the pi-conjugated system of the bilin, isolating the D-ring and dramatically blue-shifting the wavelength required to photoisomerize the C15-16 bond.

Algal Phytochromes

Blue-green photocycles are also a feature of CparGPS1 from the glaucophyte *C. paradoxa*. Like the DXCF CBCRs, CparGPS1 contains a second cysteine linkage to its bilin chromophore at C10, but the location of its second cysteine is immediately adjacent to the cysteine bound to C3 of the bilin instead of farther down the GAF domain as in DXCF-CBCRs [16].

3.2.4 Phytochromes with Altered Dark Reversion

3.3 Light-Activated Yeast Two-Hybrid

Yeast-two hybrid assays use protein-protein interaction to drive the expression of a reporter gene. The yeast Gal4 transcription factor can be split between its DNA-binding domain (GBD) and the activating domain which recruits machineries for transcription initiation (GAD). While the GBD and GAD fragments do not reconstitute a functional transcription factor when expressed in the same cell, fusion of these domains to two other proteins which do interact can promote sufficient reconstitution of functional Gal4 to produce expression of reporter genes behind Gal4-sensitive promoters.

Fusion of PhyB to GBD and PIF3 to GAD allowed photoswitching of the PhyB-PIF3 has previously been reported as a switchable yeast two-hybrid in which reporter gene expression is turn on by exposure of yeast to red light, and turned off in far red light [11]. This platform has been very successful in enabling screens to identify key residues of PhyB and PIF, both for their photoswitchable interaction (Table 3.2) as well as PIF's transcription activation activity [26]. By using selectable markers as two-hybrid reporters, survival of yeast cells can also be gated by PhyB-PIF activity. A similar selection scheme applied to directed evolution

of the Cry2-Cph blue-light activated protein interacting pair was able to successfully identify a variant of Cry2 with longer-lived interaction in dark following an activating blue light pulse [27]. This illustrates the capability of this approach to identify useful mutations even from random mutagenesis libraries of moderate size.

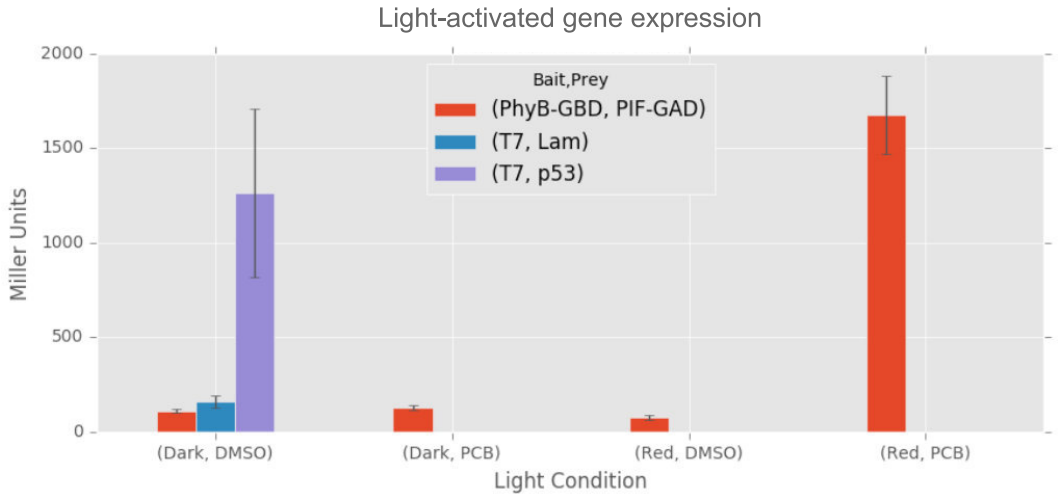

Figure 3.1: Comparing Light-Activated Yeast Two-Hybrid to Light-Independent Control T7-p53 are strongly interacting light-independent positive control, T7-Lam are non-interactive negative control. Error bars are standard deviation from 3 biological replicates.

We were able to reproduce the PhyB-PIF driven yeast two hybrid and demonstrate reporter gene expression gated by light. Optimization of expression levels of PhyB-GBD and PIF-GAD yielded the best light induction ratios (the ratio of reporter expression in red light induced cultures relative to those kept in the dark) at high expression of PhyB-GBD and low expression of PIF-GAD (Fig. 3.2)

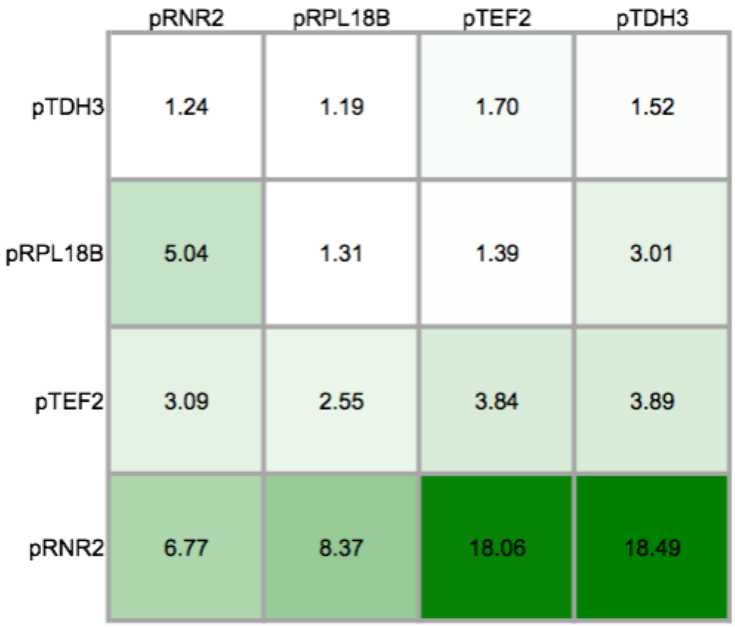

Figure 3.2: Light Induction Ratios at Varying PhyB/PIF Expression Levels
Promoter strength decreases from pTDH3, pTEF2, pRPL18B, to pRNR2.

3.3.1 Yeast Strains

Quantitative LacZ Reporter Strains

Y187 yeast (MATα, ura3-52, his3-200, ade2-101, trp1-901, leu2-3, 112, gal4Δ, met–, gal80Δ, URA3::GAL1UAS-GAL1TATA-lacZ) was obtained from Clontech.

Readout of two-hybrid reporter gene expression by fluorescence in a flow cytometer was done in the strain JF49 (MATa trp1-901 leu2-3,112 ura3-52 his3-200 gal4Δ gal80Δ LYS2::GAL1-HIS3 GAL2-ADE2 met2::GAL7-lacZ ura3:: pGal1 – yeGFP), a gift from Justin Feng. This strain was constructed by integration of a cassette containing a yeGFP reporter gene and a KanMX marker into the URA locus of strain PJ69-4a [28].

Selection Strain

The strain MaV203 (MATα; leu2-3,112; trp1-901; his3Δ200; ade2-101; cyh2R; can1R; gal4Δ; gal80Δ; GAL1::lacZ; HIS3$_{\text{UASGAL1}}$::HIS3@LYS2; SPAL10$_{\text{UASGAL1}}$::URA3), was originally developed by Marc Vidal and Jef Boeke for use in Reverse Yeast Two-Hybrid screens [29].

A GAL1 promoter in Mav203 drives expression of the LacZ gene from E. coli. The β-galactosidase gene product of LacZ enzymatically converts the colorless compound o-nitrophenyl-β-D-galactoside (ONPG) into galactose and the yellow compound o-nitrophenyl. The absorbance of o-nitrophenyl at 420nm can be measured and related quantitatively to the extent of LacZ expression and, in turn, strength of the interacting proteins responsible for reconstituting the Gal4 transcription factor.

The yeast HIS3 gene encodes imidazoleglycerol-phosphate dehydratase (IGPD), an enzyme in the yeast biochemical pathway for synthesis of histidine. MaV203 carries a HIS3 deletion and so is normally auxotrophic for histidine, but a GAL1 promoter driving HIS3 allows cells with a reconstituted Gal4 to survive in HIS-free medias. The stringency of this nutritional selection can be tuned by the addition of 3-AT, a competitive inhibitor of IGPD.

Similarly, expression of the orotidine-5'phosphate (OMP) decarboxylase enzyme encoded by the URA3 gene allows Gal4 reconstitution to rescue MaV203 cells normally auxotrophic for uracil in a uracil-free environment. In addition, OMP decarboxylase is also capable of converting relatively harmless 5-fluoroorotic acid (5-FOA) to the toxic 5-fluorouracil (5-FU). In media which contains both uracil and 5-FOA, the reconstitution of Gal4 transcription factors leads to cell death instead of growth, acting as a negative selection against bait and prey protein interaction.

3.4 Hardware

For light-stimulation of yeast in both liquid culture and on solid agar plates, a shaking incubator was outfitted with a custom arduino-controlled LED array based on an existing open-hardware design [30]. The array is built on a large printed circuit board consisting of 16 daisy-chained TLC5940 Pulse-Width Modulation (PWM) LED drivers, each controlling 16 individual LEDs arranged in banks of 4. Each bank includes one red, blue, green, and far-red LED. The LED drivers are instructed by an Arduino microconroller, allowing independent 4096 grayscale level control of each LED with 1 ms time resolution.

Each of the 64 banks can be used to provide single or multi-chromatic light to a single 15mL culture tube. Petri dishes may also be used, with their larger diameters restricting the capacity of a single board to 24 or 16 dishes of a 60mm or 100mm diameter, respectively. Culture tube or petri dish samples are embedded within holes cut to a close fit in sheets of 1" thick foam to isolate against light leakage from neighboring positions.

3.5 Light-gated Genetic Selection

MaV203 cells transformed with plasmids listed in Table 3.3 were used in survival experiments on both solid agar plates and in liquid culture to verify the correct behavior in response to selective conditions and light. Krev1 and RalGDS were used as a pair of yeast two-hybrid controls with known strengths of interaction.

3.5.1 Agar Plate Assays

Optimum light intensities and stringencies for positive and negative selection were identified on agar plates. Transformed colonies were resuspended and roughly 10^4 cells plated per

condition. Cells expressing PhyBNT-GBD and PIF3-GAD were found to survive on positive selective media only in the presence of PCB and red light stimulation. Negative selection failed to differentiate between cultures maintained in light or dark, showing ample growth under either condition. The growth of cultures on negative selection under red light was suppressed, however, for cultures which were first passed through a positive selection, suggesting a large number of PhyB/PIF transformants may have lost PhyB/PIF expression while on plasmid selection alone. Cultures passed through alternating rounds of positive selection in red light and negative selection in dark conditions consistently gave the expected patterns of growth.

3.5.2 Liquid Survival Assays

To assay the survival of yeast under positive and negative selection in liquid culture, transformed colonies were picked and incubated in media containing 15mM PCB for 4 hours, then transferred to selective media. Each culture was seeded with roughly 10^8 cells per culture in a 3mL volume of media, and grown under either continuous red light or in the dark for 4 days. The ODs of a sample of each culture was measured every 24 hours.

To identify the smallest number of cells which could be enriched under each selective condition, cultures were seeded with distinct ratios of cells carrying strong interacting pairs (KrevWT) to cells carrying non-interacting pairs(Krevm2). Under positive selection, cultures seeded with as few as $1 : 10^6$ KrevWT:Krevm2 resulted in substantial growth by day 4, while cultures seeded with Krevm2 exclusively did not grow. In negative selection, the ratios tested were reversed, with Krevm2 being doped into an excess of KrevWT due to the reversal of expected growth phenotypes; by day 4 cultures with as low as $1 : 10^6$ also showed enrichmed growth over cultures containing only KrevWT cells.

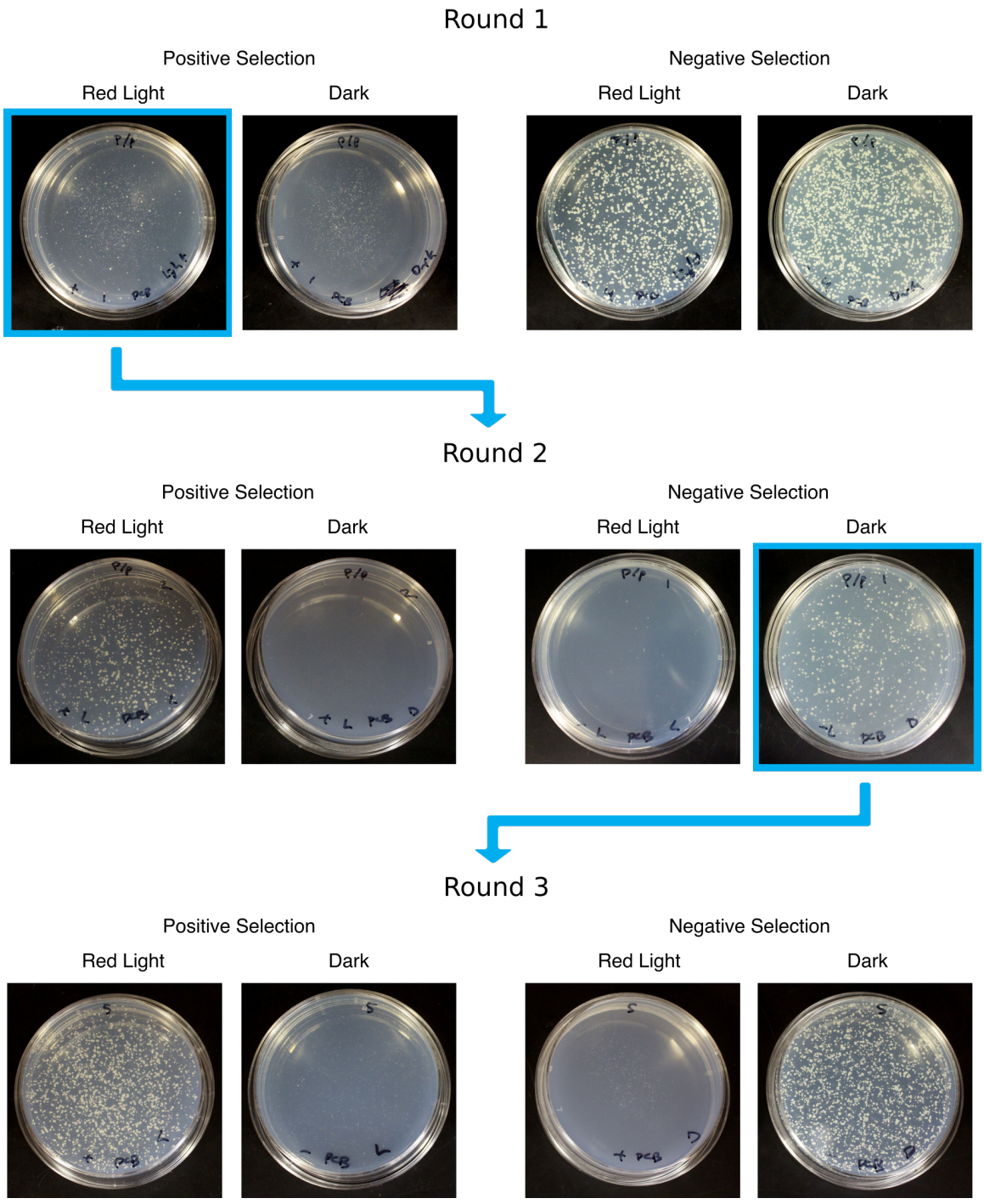

Figure 3.3: Agar Plate Selections

Three successive rounds of selection on agar plate media. Positive selection is performed on SD-LWHU with 10mM 3AT and 15mM PCB. Negative selection is performed on SD-LW with .1% 5-FOA and 15mM PCB. Colonies are picked and resuspended from a positive selection plate grown under continuous red light and plated onto negative selection. Colonies from negative selection plates growth in the dark are moved to the following positive selection.

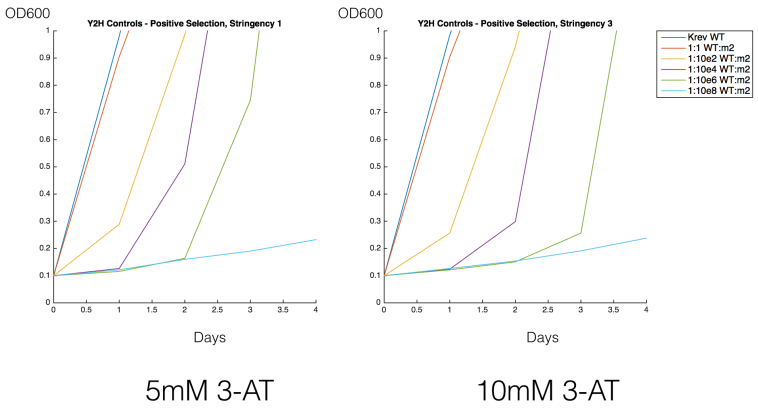

Figure 3.4: Liquid Culture Control Positive Selection
Positive selection of Y2H control strains in liquid cultures: Growth curves of cultures seeded with varying ratios of KrevWT/p53 (positive Y2H interactions) to KrevM2/p53 (non interactors). Cultures were grown in SD-LWHU with 3-AT added at the indicated concentration.

The same mock selections were carried out with cells expressing PhyB/PIF (pKA044). Under positive selection, cultures seeded with $1 : 10^4$ pKA044:Krevm2 had significant growth by day 4 under red light, while cultures with the same composition grown in the dark did not. Under negative selection, most cultures growth in the dark failed to show elevated growth relative to the corresponding red-light culture. This likely is due to the tested concentrations of 5-FOA being insufficiently strong to select against the weaker PhyB-PIF interaction compared to the strong RalGDSWT-Krev1 interaction. This also may reflect a similar behavior seen in the agar plate selections experiments, in which initial performance in the negative selection was poor, but passing cultures through a preliminary positive selection eliminated most or all of the cells exhibiting unexpected growth.

3.5.3 Library Design

Design of mutant libraries for PhyB are informed by comparing PhyB sequence and structure with the Phytochrome family proteins which exhibit blue-green photocycles, such as TePixJ from *T. elongatus* and CparGPS1 from *C. paradoxa*. Both TePixJ and CparGPS1 have

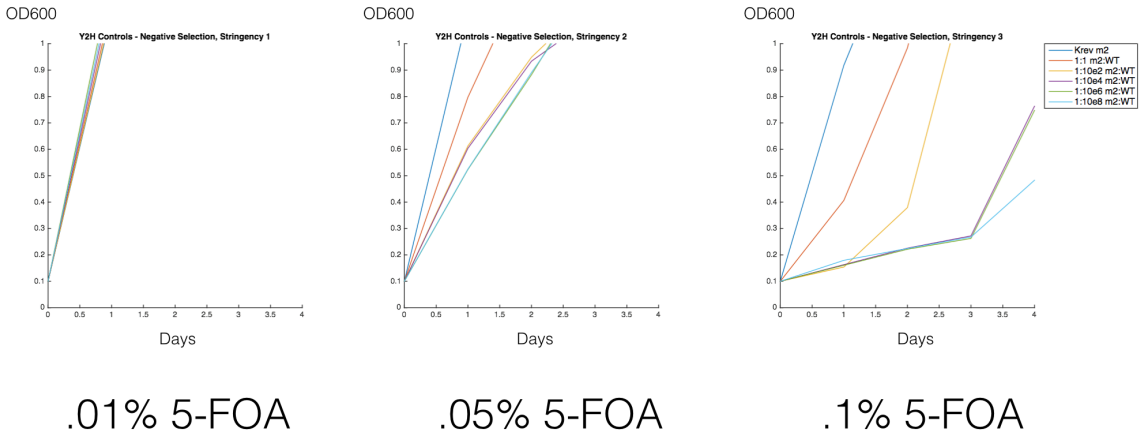

Figure 3.5: Liquid Culture Control Negative Selection

Negative selection of Y2H control strains in liquid cultures: Growth curves of cultures seeded with varying ratios of KrevM2/p53 (non interactors) to KrevWT/p53 (positive Y2H interactions). Cultures were grown in SD-LW with 5-FOA added at the indicated concentration.

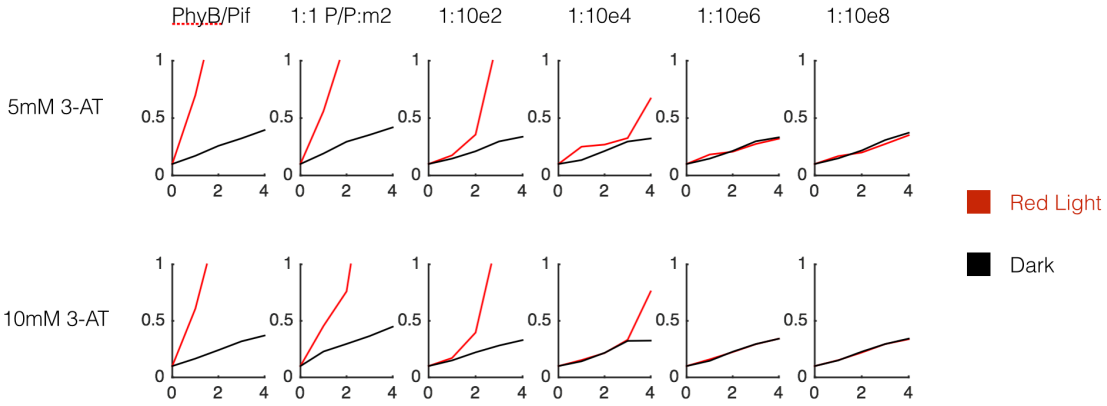

Figure 3.6: Liquid Culture PhyB/PIF wt Positive Selection

Positive selection of PhyB-PIF strains in liquid cultures: Growth curves of cultures seeded with varying ratios of PhyB-PIF to KrevM2/p53 (non interactors). Cultures were grown in SD-LWHU with 3-AT added at the indicated concentration.

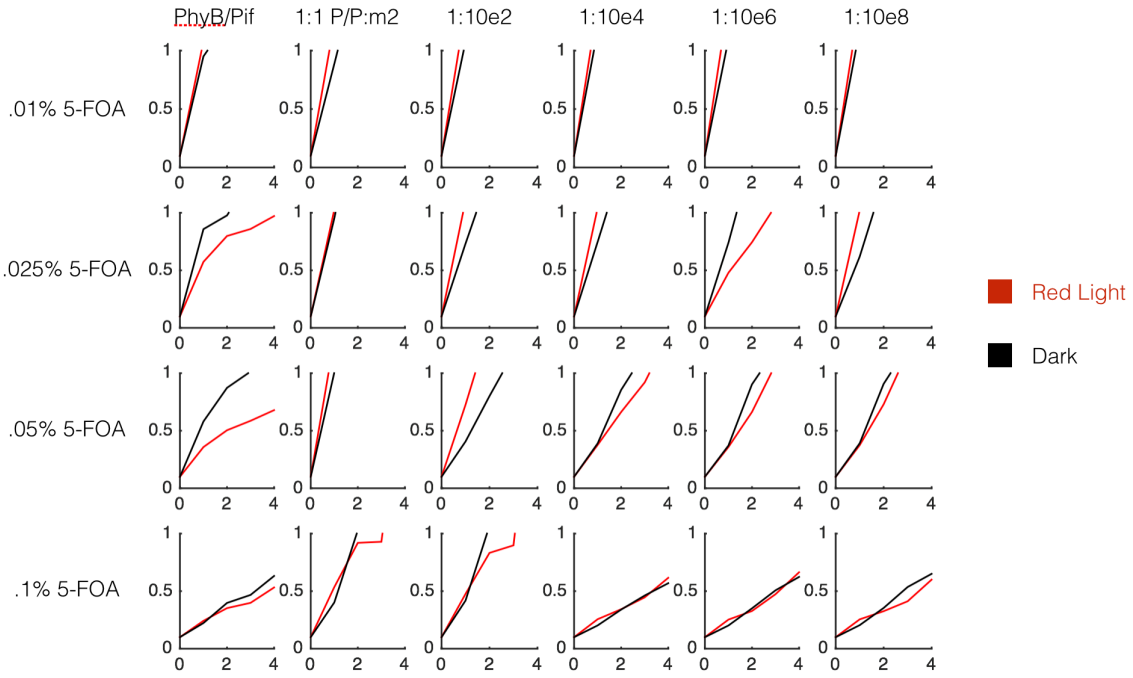

Figure 3.7: Liquid Culture PhyB/PIF wt Negative Selection

Negative selection of PhyB-PIF strains in liquid cultures: Growth curves of cultures seeded with varying ratios of PhyB-PIF to KrevWT/p53 (positive Y2H interactions). Cultures were grown in SD-LW with 5-FOA added at the indicated concentration.

blue-shifted light responses due to a second covalent linkage to the bilin chromophore, the site of the additional cysteine residue involved in this linkage vary in position in the primary sequence.

The first library constructed aims to incorporate a second cysteine immediately adjacent to the existing C357 in the GAF domain of PhyB to which PCB is bound, by substitution at H358C. The two amino acid residues immediately upstream (355,356) and downstream (359,360) of these two tandem cysteines are randomly mutated with NNK degenerate codons to allow any residue identity. The library (10^6 nucleotide diversity) is constructed by site-directed PCR replacement of the 355-360 region in PhyB, and expanded in E. coli. Design and construction of this CysB library was performed by Kamran Ali.

The library is the prepped from E. coli and transformed into MaV203 yeast using standard LiAC-based transformation.

3.5.4 Library Hits and Follow-up Characterizations

A small scale positive selection experiment was carried out on agar plates. Cells transformed with wild-type PhyB/PIF were plated on SD-LHU plates containing 15mM PCB and 10mM 3-AT. Five different light conditions were tested: red light, dark, and blue light at three different intensities. Roughly $5 * 10^5$ cells were plated per condition.

After three days, roughly 50 colonies were found in each condition, suggesting that the surviving colonies represent PhyB mutants which bind PIF constitutively, independent of light condition. All colonies were picked and a subset sequenced from each condition. Sequences are reported in Table 3.4 as protein translations of the mutated region in the format XXCC*XX, with C* being the introduced second cysteine.

Of note, members sharing the same amino acid sequence shared the same codon representation, while codon representations for the same amino acid different across different groups. Since our yeast transformation only produced 10^5 transformants, we do not expect to have fully covered our library in this initial selection, and the lack of codon degeneracy within members sharing a primary amino acid sequence suggests that significant clonal expansion occurred during recovery of library transformants in liquid culture.

All colonies were transfered to 4 liquid culture conditions: positive and negative selection, with and without PCB. No growth was seen for any members in this follow up negative selection except a small number of colonies which had originally survived positive selection under red light. All of these colonies sequenced as wild-type members. Interesting, all other colonies were found to grow in positive selection with or without PCB, indicating the TPCCWL, TPCCWI, and MPCCVG variants are locked in a PIF-binding conformation even without chromophore bound in the GAF pocket. This can be verified for each variant by re-transforming the mutant in question and performing one of the assays for chromophore binding outlined below.

3.6 Response Speed of Light-activated Gene Expression

Multichromatic control of gene expression has been demonstrated through combination of optogenetic systems with sensitivities to different light wavelengths [31]. In experiments seeking to both control gene expression and perform live imaging over time, light wavelengths used for optogenetic control cannot also be used as excitation sources for fluorescence. Multiplexing control information within a single spectral channel is then attractive to free up optical bandwidth for live readouts of cell state.

Natural processes are capable of decoding different temporal presentations of the same signal into distinct responses. In many of these, such as gene expression regulated by NF-Kβ in response to calcium influxes [32, 33] or T-cell activation by extracellular ligands [34], protein translocation plays a role in shaping response speed.

Synthetic control of protein translocation is also a useful synthetic tool; for example, engineered nuclear localization has been applied to produce reporters for kinase activity [35]. Along similar lines, optogenetic control of nuclear localization has been demonstrated through a number of approaches. These include embedding a photocaged unnatural amino acid residue within a nuclear localization sequence [36], using light-driven protein structural rearrangements to unveil a NLS [37, 38], dimerization of a cytoplasmically localized component to an NLS-containing partner [39, 40].

We hypothesized that subcellular compartmentalization of PhyB and PIF components could alter the speed with which gene activation could be produced in response to light-induced PhyB-PIF interaction. A scheme relying on nuclear localization to introduce delays in transducing PhyB-PIF interaction to transcriptional activation is outlined in Figure 3.8. In yeast, translation of PhyB and PIF fusions proteins is initiated in the cytoplasm. Presence of nuclear localization signals in both translated protein recruit importins resulting in the complex being transported across the nuclear envelope into the nucleus. We hypothesized that altering the localization of one half of the twp-hybrid components, light-activated interaction of PhyB and PIF would have to be sustained through nuclear co-import. In this way, activating light pulses shorter than the time required for translocation would not successfully activate gene expression.

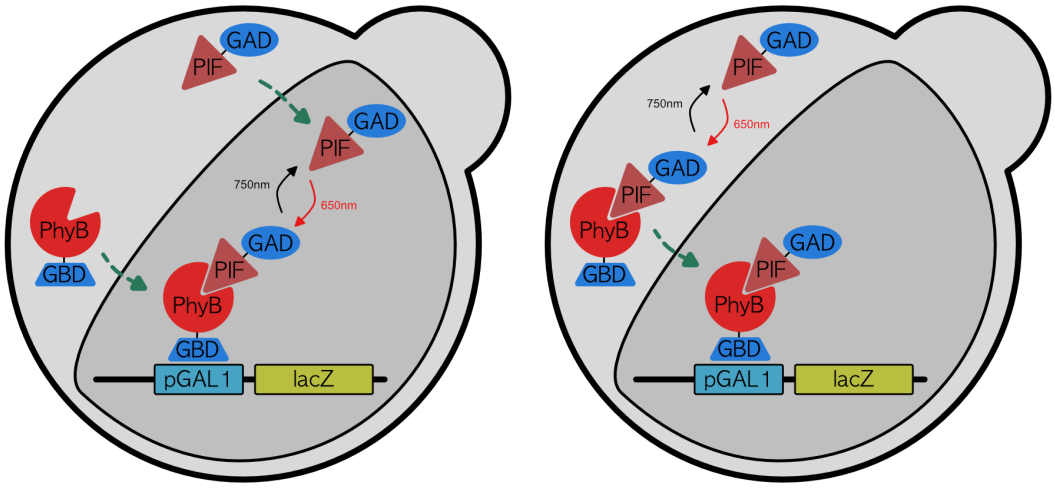

Figure 3.8: Schematic of Alternative PhyB-PIF Subcellular Localizations
Left: "Nuclear-Nuclear" - Light induction dimerizes PhyB and PIFs already present in nucleus to produce immediate transcription. Right: "Nuclear-Cytoplasmic" - Light induction initiates and must persist throughout nuclear import of PIF for transcription to occur.

3.6.1 Modifying PhyB/PIF Subcellular Localization

Because nucleocytoplasmic shuttling of phytochromes is believed to be important to fine-tuning their light-mediated responses in Arabidopsis [41], we felt it a safe assumption that similar shuttling (with a NLS-carrying protein supporting the import of an interacting partner carrying no import signal) would be possible in other hosts as well. This was recently shown in mammalian cells [40], but not in yeast.

In the original formulation of the light-activated yeast-hybrid, PhyB and PIF's fusion partners (GBD and GAD, respectively) both contain active NLS sequences. GBD contains the natural NLS found in the full Gal4 transcription factor, while the GAD fragment has a synthetic NLS from the SV40 virus fused on its N-termini. Removal of the SV40 NLS from GAD returns its localization to the cytoplasm. The NLS of the GBD is not easily removed or mutated away, however, due to its position in the protein, sharing a number of residues with the DNA-binding motif of GBD [42]. Therefore it is easier in practice to control the lo-

calization of GAD between nuclear and cytoplasmic compartment by including or excluding the SV40 NLS.

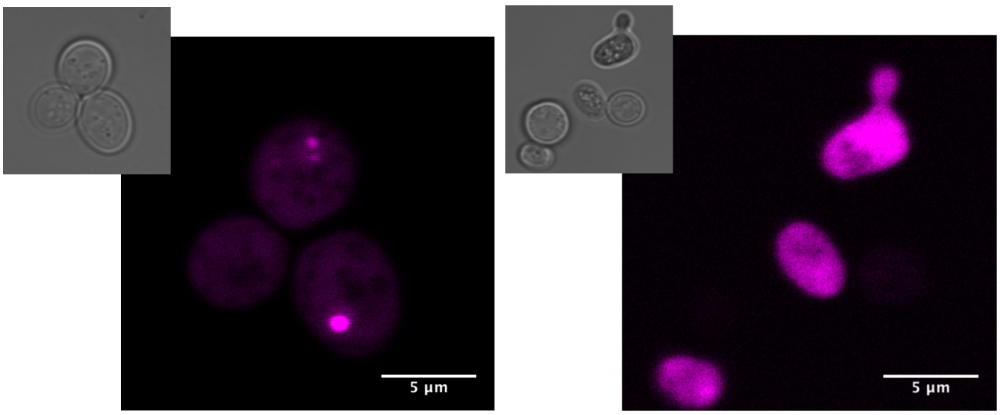

Figure 3.9: Epifluorescence imaging of PIF localization
Left: PIF-GAD-mRuby2. Right: PIFΔNLS-GADΔNLS-mRuby2. Insets are hoffman modulation contrast images

We first engineered variants of the PIF-GAD fusion that either localized to cytoplasm instead of the nucleus, and confirmed this by live imaging of an included a mRuby2 fluorescent protein tag (Fig. 3.9).

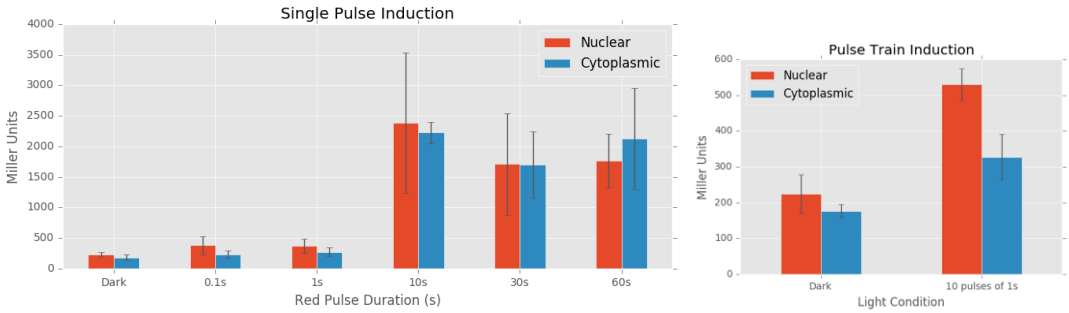

Figure 3.10: Yeast-two hybrid activity elicited by varying pulse durations.
Left: Repsonses to single light pulse. Right: responses to trains of short pulses. 10 repeats of 1 sec red light followed by 120 seconds in the dark. Scalebars are all standard deviation

Using yeast strains co-transformed with PhyB-GBD and PIFΔNLS-GADΔNLS, we confirmed that red light stimulation (10 μW/cm^2) is able to produce reporter gene expression. Unfortunately, there was not found to be any single red light activating pulse duration which produced differential responses between the two schemes (Nuclear-Nuclear vs. Nuclear-Cytoplasmic).

While a 1 second pulse of red light was insufficient to produce reporter expression above background, 10 individual 1 second pulses, each separated by 120 seconds of dark, produced a measurable increase in expression from yeast with the Nuclear-Nuclear PhyB-PIF system. Though not statistically significant, the slightly lower levels of reporter expression produced in Nuclear-Cytoplasmic strains suggests that controlling rate at which PhyB-PIF pairs dissociates (with possible subsequent nuclear export of PIF) in the absence of light could also be useful to altering the overal responsiveness of the system to different light pulse patterns.

3.7 Future Work

In the current selection strategy, successful PhyB mutants likely must meet multiple criteria: to form haloproteins with PCB, establish a second covalent linkage to produce a hypsochromic shift in the chromophore's excitation, and produce a similar conformational change in response to photoisomerization of the chromophore. Achieving all of these simultaneously might potentially require changes outside the chromophore binding site of PhyB. With limitations on library size we were able to transform in yeast, it may be more reasonable to target individual functions stepwise, such as first selecting only for the ability incorporate PCB, using successful candidates as the starting point for future libraries. Alternatively, another approach would be to target PhyB variants which are capable of incorporating other bilin chromophores with photocycles sufficiently shifted from PCB. Bilirubin, for example, is highly similar in structure to that of PCB with a saturated C10-C11 bond and exhibits photoreversible isomzerization around 420-530nm photocycles (a feature which is leveraged in phototherapy treatments for jaundice [43]).

Alternate approaches could be pursued to alter PhyB-PIF response speed. For example, one could employ PhyB variants with different rates of dark reversion, such as the fast-reverting E812K mutant and the slow-reverting G564E, in combination with light pulse trains with

varying duty cycles. Even without modification of subcellular localization, it may be possible to achieve differences in activation as the duration of "off" periods between activating "on" light pulses. Many other changes might also help in better separating fast and slow responding PhyB-PIF Y2H schemes. These include selecting promoters with different transfer functions [44], tuning protein degradation rates[45], and the addition of non-functional PhyB or PIF binding partners to tune the rate of functional interactions through competition [46]. The tremendous number of parameters which could be tuned suggests the best course could be to first establish a mathematical model of light-activated gene expression and systematically adjust one parameter at a time experimentally. In this manner unknown parameters can be estimated, and the model used to guide further engineering efforts; previous work has shown this to be effective for other two-component optogenetic controllers in E coli [47].

Optogenetic controllers of transcription with fast on and off kinetics can also be used to measure dynamics of the transcriptional process itself [48]. With additional characterization, the PhyB-PIF might also be applied similarly to measurement of the rates of fundamental biological processes.

3.8 Methods

3.8.1 Agar Plate Survival Assay

The yeast strain MaV203 (MATα; leu2-3,112; trp1-901; his3Δ200; ade2-101; cyh2R; can1R; gal4Δ; gal80Δ; GAL1::lacZ; HIS3UASGAL1::HIS3@LYS2; SPAL10 UASGAL1::URA3) was obtained from Invitrogen. Yeast were transformed according to the Clontech Yeast Protocols Handbook. Fresh colonies transformed with PhyB(NT)-GBD and PIF6-GAD were picked into SD(–L) medium supplemented with 25 μM PCB and cultured for 3 hours in darkness,

then spread onto either SD(–LHU) with 10 μM 3-AT and 25 μM PCB for positive selections or SD(-L) with , either in continuous red light (10 $\mu W/cm^2$) or darkness for 3 days.

Because PCB degrades at elevated temperatures, care must be taken to allow agar to cool to about 65 $^\circ$C before supplementing with PCB. Plates should be poured in the dark on the same day cells are plated.

3.8.2 Liquid Culture Survival Assay

Fresh colonies transformed with PhyB(NT)-GBD and PIF6-GAD were picked into SD(–L) medium supplemented with 25 μM PCB and cultured for 12 hours in darkness, then back diluted 1:1000 into SD(–L) 25 μM PCB, either in continuous red light (10 $\mu W/cm^2$)or darkness for 4 days.

3.8.3 Light-activated Quantitative LacZ Assay

This protocol, adapted from [49] covers the steps of a typical light-induced gene expression experiment in a S. cerevisiae host. Parameters and reagents given here are specific to the PhyB-PIF Y2H-based light responsive system and ONPG-based LacZ assay for expression, but the overall scheme can be applied to other light inducible systems and reporter assays easily.

The entire protocol spans 2 days, with the key light induction step and assaying taking place through most of the second day.

Purpose

This protocol covers the steps of a typical light-induced gene expression experiment in a S. cerevisiae host. Parameters and reagents given here are specific to the PhyB-PIF Y2H-based light responsive system and ONPG-based LacZ assay for expression, but the overall scheme can be applied to other light inducible systems and reporter assays easily.

The entire protocol spans 2 days, with the key light induction step and assaying taking place through most of the second day.

Materials

- Streak plate of candidate yeast clones (plate should be fresh: $< 1\ month$)
- Appropriate SD liquid medium
- YPD
- 12 mM PCB in DMSO
- Pierce/ThermoFisher Y-PERS reagent
- 4 mM ONPG Solution

Procedure

Day 0

1. **Inoculate** 5 min 16 hour incubation

    - For each clone to be assayed, pick a **single fat colony** into **2 mL** of the appropriate SD media
    - Grow overnight **16 hours**, shaking at **30°C**

2. **Design Light Program** 10 min

    - Use XYZ program to assemble an Arduino sketch with a light box program for the desired stimulations patterns

Day 1

1. **Backdilute Cultures**

    15 min

    - For each 96-well block of overnight cultures, prepare the below **4x 96-well blocks**, with **800 uL of media** per well
        - **A**: YPD + PCB
        - **B**: YPD + PCB
        - **C**: YPD + DMSO
        - **D**: YPD + DMSO
    - Inoculate each well with **200uL** of overnight culture

2. **Light Induction**

    15 min

    3 hour incubation

    - Expose Plates **A** and **C** to **light**

        A "standard" exposure is 10 minutes of continuous red light

- Leave Plates **B** and **D** in the **dark**
- Collect all blocks and incubate shaking at **30°C** for **3 hours** in the **dark**

3. **Prep LacZ Assay Plates**

   5 min

   - Prepare **OD600 Plate(s)**
     - Transfer in **200 uL** of each sample culture well
   - Prepare **OD420/550 Plate(s)**
     - Add **100 uL** of **4 mM ONPG** solution in each well
     - Tramsfer in **100 uL** of each sample culture from the **OD600 Plate(s)**

4. **Read Assay Plates - Initial**

   5 min

   0.5-3 hours

   - On the Tecan m200 Plate reader, read all sample wells on the **OD 600 Plate(s)**:
     - Plate Type: Costar 96 Flat Transparent
     - Absorbance: **600nm** (other default settings ok)
   - Incubate **OD420/550 Plate(s)** at **37C** until color change is visible (typically 30 to 90 minutes)

5. **Read Assay Plates - Final**

   5 min

   - On the Tecan m200 Plate reader, read all sample wells on the **OD 600 Plate(s)**:
     - Plate Type: Costar 96 Flat Transparent
     - Absorbance 1: **420nm** (other default settings ok)
     - Absorbance 2: **550nm** (other default settings ok)
   - Transfer all data and shut off plate reader

Table 3.2: Phytochrome B Mutants identified in Yeast Two-hybrid screens

PCB: + indicates covalent adduct formation with PCB, - indicates no incorporation of PCB. DS: + indicates bathychromic shift spectra measured, - indicates hypsochromic shift. DR: + indicates faster dark reversion from pfr to pr, - indicates slower dark reversion.

Mutant	Domain	Phenotype	PCB	DS	DR	Phenotype Notes	First Reported
Y276H	GAF	GOF	+		−−	Consitutive binding to PIF3, PCB dependent. Fluorescent	Su, Lagarias 2007 [17]
E812K	PAS2	LOF			++	Rapid Dark Reversion	Elich, Chory 1997 [18]
H283Y	GAF	LOF			+		Elich, Chory 1997 [18]
D64N	N-term	LOF	+	+	+	Long hypototyl, severe or complete loss of phyB activity	Oka, Quail, Nagatani 2008 [19]
R110Q	PAS	LOF	+	+	+	Long hypototyl, severe or complete loss of phyB activity	Oka, Quail, Nagatani 2008 [19]
G111D	PAS	LOF	+	+	+	Long hypototyl, severe or complete loss of phyB activity	Oka, Quail, Nagatani 2008 [19]
G112D	PAS	LOF	+	+	+	Signal transfer mutant, intermediate hypocotyl, insensitive to light fluence	Oka, Quail, Nagatani 2008 [19]
G118R	PAS	LOF	–	nd	nd	Long hypototyl, severe or complete loss of phyB activity	Krall, Reed 2000; Chen, Chory 2003 [20, 21]
S134G	PAS	LOF	–	nd	nd	Intermediate hypocotyl length sensitive to light fluence, poor binding to PIF3	Krall, Reed, 2000 [20]
P149L	PAS	LOF	+	+	+	Signal transfer mutant, intermediate hypocotyl, insensitive to light fluence	Oka, Quail, Nagatani 2008 [19]
I208T	PAS		+	+	+		Krall, Reed, 2000 [20]
H283T	GAF		+	+	-		Reed, Chory 1993 [22]
G284E	GAF	LOF	-	-	nd	Intermediate hypocotyl, sensitive to light fluence	Oka, Quail, Nagatani 2008 [19]
P304L	GAF	LOF	+	+	+	Intermediate hypocotyl, sensitive to light fluence	Oka, Quail, Nagatani 2008 [19]
P309L	GAF	LOF	-	-	nd	Long hypototyl, severe or complete loss of phyB activity	Oka, Quail, Nagatani 2008 [19]
R313K	GAF	LOF	+	+	-	Intermediate hypocotyl, sensitive to light fluence	Oka, Quail, Nagatani 2008 [19]
R322Q	GAF	LOF	+	-	−−	Intermediate hypocotyl, sensitive to light fluence	Oka, Quail, Nagatani 2008 [19]
C327Y	GAF		+	+	-		Chen, Chory 2003 [21]
R352K	GAF	LOF	+	+	+	Signal transfer mutant, intermediate hypocotyl, insensitive to light fluence	Oka, Quail, Nagatani 2008 [19]
S370F	GAF	LOF	–	-	nd	Long hypototyl, severe or complete loss of phyB activity	Oka, Quail, Nagatani 2008 [19]
A372T	GAF		+	-	−−		Chen, Chory 2003 [21]
V401I	GAF	LOF	+	+	-	Intermediate hypocotyl, sensitive to light fluence	Oka, Quail, Nagatani 2008 [19]
G564A	PHY		+	+	-	Faster photoreversion	Oka, Tokutomi 2004; Kretsch, Schafer 2000 [23, 24]
S584F	PHY	LOF	+	-	−−	Intermediate hypocotyl, sensitive to light fluence	Oka, Quail, Nagatani 2008 [19]
A587T	PHY		+	+	-		Chen, Chory 2003 [21]
G564E	PHY	GOF	+		−−	No photoreversion, slow dark reversion, hypersensitivity	Kretsch, Schafer 2000 [24]
S86D			+			Phosphomimic, faster dark reversion, enhanced R sensitivity	Kretsch, Schafer 2001 [25]
G576E	PHY	LOF	nd	nd	nd		Schafer, unpublished
P581L	PHY	LOF	nd	nd	nd		Schafer, unpublished
A719V	PAS1	LOF	nd	nd	nd		Schafer, unpublished
A750V	PAS1	LOF	nd	nd	nd		Schafer, unpublished
G515N	PHY	GOF	nd	nd	nd	Unknown phenotype, likely constitutive active with PCB	Schafer, unpublished
G565S	PHY	GOF	nd	nd	nd	Unknown phenotype, likely constitutive active with PCB	Schafer, unpublished

Table 3.3: List of plasmids used to transform MaV203

Plasmid	Product Expressed	Selective Marker
pEXP22-RalGDSwt	RalGDSwt-GAD (strong interaction with Krev1)	Trp
pEXP22-RalGDSm1	RalGDSm1-GAD (weak interaction with Krev1)	Trp
pEXP22-RalGDSm2	RalGDSm2-GAD (no interaction with Krev1)	Trp
pEXP32-Krev1	Krev1-GBD	Leu
pGBD-PhyBNT	PhyB-GBD	Trp
pGAD-PIF3	PIF3-GAD	Leu
pKA044	PhyBNT-GBD and PIF3-GAD	Leu

Table 3.4: Colonies sequenced from each light condition

Sequence Identity	Dark	Red	Blue, Low	Blue, Medium	Blue, High
HGCHSQ (wt)	-	4	-	-	-
TPCCWL	4	2	4	5	5
TPCCWI	1	-	-	-	2
MGCCVG	1	1	1	2	1
Total sequenced:	6	7	5	7	8

Bibliography

[1] J. E. Toettcher, C. A. Voigt, O. D. Weiner, and W. A. Lim, "The promise of optogenetics in cell biology: interrogating molecular circuits in space and time.," *Nature methods*, vol. 8, no. 1, pp. 35–38, 2011.

[2] E. R. Ballister, C. Aonbangkhen, A. M. Mayo, M. a. Lampson, and D. M. Chenoweth, "Localized light-induced protein dimerization in living cells using a photocaged dimerizer," *Nature Communications*, vol. 5, p. 5475, nov 2014.

[3] A. S. Baker and A. Deiters, "Optical Control of Protein Function through Unnatural Amino Acid Mutagenesis and other Optogenetic Approaches.," *ACS chemical biology*, may 2014.

[4] M. J. Kennedy, R. M. Hughes, L. a. Peteya, J. W. Schwartz, M. D. Ehlers, and C. L. Tucker, "Rapid blue-light-mediated induction of protein interactions in living cells.," *Nature methods*, vol. 7, pp. 973–5, dec 2010.

[5] L. J. Bugaj, A. T. Choksi, C. K. Mesuda, R. S. Kane, and D. V. Schaffer, "Optogenetic protein clustering and signaling activation in mammalian cells.," *Nature methods*, vol. 10, pp. 249–52, mar 2013.

[6] X. X. Zhou, H. K. Chung, A. J. Lam, and M. Z. Lin, "Optical control of protein activity by fluorescent protein domains.," *Science (New York, N.Y.)*, vol. 338, pp. 810–4, nov 2012.

[7] M. Yazawa, A. M. Sadaghiani, B. Hsueh, and R. E. Dolmetsch, "Induction of protein-protein interactions in live cells using light.," *Nature biotechnology*, vol. 27, no. 10, pp. 941–945, 2009.

[8] A. Levskaya, O. D. Weiner, W. a. Lim, and C. a. Voigt, "Spatiotemporal control of cell signalling using a light-switchable protein interaction.," *Nature*, vol. 461, pp. 997–1001, oct 2009.

[9] J. J. Tabor, A. Levskaya, and C. a. Voigt, "Multichromatic control of gene expression in Escherichia coli.," *Journal of molecular biology*, vol. 405, pp. 315–24, jan 2011.

[10] K. Müller, R. Engesser, J. Timmer, M. D. Zurbriggen, and W. Weber, "Orthogonal Optogenetic Triple-Gene Control in Mammalian Cells.," *ACS synthetic biology*, oct 2014.

[11] S. Shimizu-Sato, E. Huq, J. M. Tepperman, and P. H. Quail, "A light-switchable gene promoter system.," *Nature biotechnology*, vol. 20, pp. 1041–4, oct 2002.

[12] E. S. Burgie, A. N. Bussell, J. M. Walker, K. Dubiel, and R. D. Vierstra, "Crystal structure of the photosensing module from a red/far-red light-absorbing plant phytochrome.," *Proceedings of the National Academy of Sciences of the United States of America*, vol. 2014, jun 2014.

[13] E. S. Burgie, J. M. Walker, G. N. Phillips, and R. D. Vierstra, "A photo-labile thioether linkage to phycoviolobilin provides the foundation for the blue/green photocycles in DXCF-cyanobacteriochromes.," *Structure (London, England : 1993)*, vol. 21, pp. 88–97, jan 2013.

[14] N. C. Rockwell and J. C. Lagarias, "A brief history of phytochromes.," *Chemphyschem : a European journal of chemical physics and physical chemistry*, vol. 11, pp. 1172–80, apr 2010.

[15] L.-O. Essen, J. Mailliet, and J. Hughes, "The structure of a complete phytochrome sensory module in the Pr ground state.," *Proceedings of the National Academy of Sciences of the United States of America*, vol. 105, pp. 14709–14, sep 2008.

[16] N. C. Rockwell, S. S. Martin, A. G. Gulevich, and J. C. Lagarias, "Conserved phenylalanine residues are required for blue-shifting of cyanobacteriochrome photoproducts.," *Biochemistry*, vol. 53, pp. 3118–30, may 2014.

[17] Y.-s. Su and J. C. Lagarias, "Light-Independent Phytochrome Signaling Mediated by Dominant GAF Domain Tyrosine Mutants of Arabidopsis Phytochromes in Transgenic Plants," *the Plant Cell Online*, vol. 19, no. 7, pp. 2124–2139, 2007.

[18] T. D. Elich and J. Chory, "Biochemical characterization of Arabidopsis wild-type and mutant phytochrome B holoproteins.," *The Plant cell*, vol. 9, no. December, pp. 2271–2280, 1997.

[19] Y. Oka, T. Matsushita, N. Mochizuki, P. H. Quail, and A. Nagatani, "Mutant Screen Distinguishes between Residues Necessary for Light-Signal Perception and Signal Transfer by Phytochrome B," *PLoS Genetics*, vol. 4, no. 8, p. e1000158, 2008.

[20] L. Krall and J. W. Reed, "The histidine kinase-related domain participates in phytochrome B function but is dispensable.," *Proceedings of the National Academy of Sciences of the United States of America*, vol. 97, no. 14, pp. 8169–8174, 2000.

[21] M. Chen, R. Schwab, and J. Chory, "Characterization of the requirements for localization of phytochrome B to nuclear bodies.," *Proceedings of the National Academy of Sciences of the United States of America*, vol. 100, no. 24, pp. 14493–14498, 2003.

[22] J. W. Reed, P. Nagpal, D. S. Poole, M. Furuya, and J. Chory, "Mutations in the gene for the red/far-red light receptor phytochrome B alter cell elongation and physiological responses throughout Arabidopsis development.," *The Plant cell*, vol. 5, no. 2, pp. 147–157, 1993.

[23] Y. Oka, T. Matsushita, N. Mochizuki, T. Suzuki, and S. Tokutomi, "Functional Analysis of a 450 – Amino Acid N-Terminal Fragment of Phytochrome B in Arabidopsis," *The Plant cell*, vol. 16, no. August, pp. 2104–2116, 2004.

[24] C. Büche, C. Poppe, E. Schäfer, and T. Kretsch, "eid1: a new Arabidopsis mutant hypersensitive in phytochrome A-dependent high-irradiance responses.," *The Plant cell*, vol. 12, no. 4, pp. 547–558, 2000.

[25] M. Dieterle, "EID1, an F-box protein involved in phytochrome A-specific light signaling," *Genes & Development*, vol. 15, pp. 939–944, apr 2001.

[26] J. C. Dalton, U. Bätz, J. Liu, G. L. Curie, and P. H. Quail, "A Modified Reverse One-Hybrid Screen Identifies Transcriptional Activation Domains in PHYTOCHROME-INTERACTING FACTOR 3," *Frontiers in Plant Science*, vol. 7, no. June, pp. 1–15, 2016.

[27] A. Taslimi, B. Zoltowski, J. G. Miranda, G. P. Pathak, R. M. Hughes, and C. L. Tucker, "Optimized second-generation CRY2-CIB dimerizers and photoactivatable Cre recombinase," *Nature Chemical Biology*, vol. 12, pp. 425–430, jun 2016.

[28] J. Feng, B. W. Jester, C. E. Tinberg, D. J. Mandell, M. S. Antunes, R. Chari, K. J. Morey, X. Rios, J. I. Medford, G. M. Church, S. Fields, and D. Baker, "A general strategy to construct small molecule biosensors in eukaryotes," *eLife*, vol. 4, no. DECEMBER2015, pp. 1–23, 2015.

[29] M. Vidal, R. K. Brachmann, a. Fattaey, E. Harlow, and J. D. Boeke, "Reverse two-hybrid and one-hybrid systems to detect dissociation of protein-protein and DNA-protein interactions.," *Proceedings of the National Academy of Sciences of the United States of America*, vol. 93, pp. 10315–20, sep 1996.

[30] E. J. Olson, L. A. Hartsough, B. P. Landry, R. Shroff, and J. J. Tabor, "Characterizing bacterial gene circuit dynamics with optically programmed gene expression signals.," *Nature methods*, vol. 11, pp. 449–55, apr 2014.

[31] K. Müller, R. Engesser, S. Schulz, T. Steinberg, P. Tomakidi, C. C. Weber, R. Ulm, J. Timmer, M. D. Zurbriggen, and W. Weber, "Multi-chromatic control of mammalian gene expression and signaling.," *Nucleic acids research*, vol. 41, p. e124, jul 2013.

[32] L. Ashall, C. A. Horton, D. E. Nelson, P. Paszek, C. V. Harper, K. Sillitoe, S. Ryan, D. G. Spiller, J. F. Unitt, D. S. Broomhead, D. B. Kell, D. A. Rand, V. Sée, and M. R. White, "Pulsatile stimulation determines timing and specificity of NF-κB-dependent transcription," *Science*, vol. 324, pp. 242–246, apr 2009.

[33] S. Zambrano, I. de Toma, A. Piffer, M. E. Bianchi, and A. Agresti, "NF-κB oscillations translate into functionally related patterns of gene expression," *eLife*, vol. 5, p. e09100, jan 2016.

[34] P. A. van der Merwe and O. Dushek, "Mechanisms for T cell receptor triggering.," *Nature reviews. Immunology*, vol. 11, no. 1, pp. 47–55, 2011.

[35] S. Regot, J. J. Hughey, B. T. Bajar, S. Carrasco, and M. W. Covert, "High-sensitivity measurements of multiple kinase activities in live single cells," *Cell*, vol. 157, no. 7, pp. 1724–1734, 2014.

[36] A. Gautier, D. P. Nguyen, H. Lusic, W. An, A. Deiters, and J. W. Chin, "Genetically Encoded Photocontrol of Protein Localization in Mammalian Cells," *Journal of the American Chemical Society*, vol. 132, pp. 4086–4088, mar 2010.

[37] D. Niopek, D. Benzinger, J. Roensch, T. Draebing, P. Wehler, R. Eils, and B. Di Ventura, "Engineering light-inducible nuclear localization signals for precise spatiotemporal control of protein dynamics in living cells," *Nature Communications*, 2014.

[38] H. Yumerefendi, D. J. Dickinson, H. Wang, S. P. Zimmerman, J. E. Bear, B. Goldstein, K. Hahn, and B. Kuhlman, "Control of protein activity and cell fate specification via light-mediated nuclear translocation," *PLoS ONE*, vol. 10, no. 6, pp. 1–19, 2015.

[39] H. M. Beyer, S. Juillot, K. Herbst, S. L. Samodelov, K. Müller, W. W. Schamel, W. Römer, E. Schäfer, F. Nagy, U. Strähle, W. Weber, and M. D. Zurbriggen, "Red Light-Regulated Reversible Nuclear Localization of Proteins in Mammalian Cells and Zebrafish," *ACS Synthetic Biology*, 2015.

[40] N. Noda and T. Ozawa, "Light-controllable Transcription System by Nucleocytoplasmic Shuttling of a Truncated Phytochrome B," *Photochemistry and Photobiology*, pp. 1–6, 2018.

[41] C. Klose, A. Viczián, S. Kircher, E. Schäfer, and F. Nagy, "Molecular mechanisms for mediating light-dependent nucleo/cytoplasmic partitioning of phytochrome photoreceptors," *New Phytologist*, vol. 206, no. 3, pp. 965–971, 2015.

[42] J. P. S. Makkerh, C. Dingwall, and R. A. Laskey, "Comparative mutagenesis of nuclear localization signals reveals the importance of neutral and acidic amino acids," *Current Biology*, vol. 6, no. 8, pp. 1025–1027, 1996.

[43] J. F. Ennever, A. F. McDonagh, and W. T. Speck, "Phototherapy for neonatal jaundice: Optimal wavelengths of light," *The Journal of Pediatrics*, vol. 103, no. 2, pp. 295–299, 1983.

[44] J. Blazeck, R. Garg, B. Reed, and H. S. Alper, "Controlling promoter strength and regulation in Saccharomyces cerevisiae using synthetic hybrid promoters," *Biotechnology and Bioengineering*, 2012.

[45] A. Bachmair, D. Finley, and A. Varshavsky, "In vivo half-life of a protein is a function of its amino-terminal residue," *Science*, 1986.

[46] L. Potvin-Trottier, N. D. Lord, G. Vinnicombe, and J. Paulsson, "Synchronous long-term oscillations in a synthetic gene circuit," *Nature*, vol. 538, no. 7626, pp. 514–517, 2016.

[47] E. J. Olson, C. N. Tzouanas, and J. J. Tabor, "A photoconversion model for full spectral programming and multiplexing of optogenetic systems," *Molecular Systems Biology*, 2017.

[48] M. Rullan, D. Benzinger, G. W. Schmidt, A. Milias-Argeitis, and M. Khammash, "An Optogenetic Platform for Real-Time, Single-Cell Interrogation of Stochastic Transcriptional Regulation," *Molecular Cell*, vol. 70, no. 4, pp. 745–756.e6, 2018.

[49] N. Möckli and D. Auerbach, "Quantitative β-galactosidase assay suitable for high-throughput applications in the yeast two-hybrid system," *BioTechniques*, vol. 36, no. 5, pp. 872–876, 2004.